Earth-Science Reviews 209 (2020) 103329

Contents lists available at ScienceDirect

Earth-Science Reviews

journal homepage: www.elsevier.com/locate/earscirev

Review Article

# Migration controls extinction and survival patterns of foraminifers during the Permian-Triassic crisis in South China

Xiaokang Liu[a], Haijun Song[a,*], David P.G. Bond[b], Jinnan Tong[a], Michael J. Benton[c]

[a] State Key Laboratory of Biogeology and Environmental Geology, School of Earth Sciences, China University of Geosciences, Wuhan 430074, China
[b] Department of Geography, Geology and Environment, University of Hull, Hull HU6 7RX, UK
[c] School of Earth Sciences, University of Bristol, Bristol BS8 1RJ, UK

ARTICLE INFO

*Keywords:*
Foraminifera
Spatial-temporal evolution
Selective extinction
Survival strategy
Deep-ward migration

ABSTRACT

The Permian-Triassic mass extinction, the greatest biotic crisis in Earth history, triggered the complete replacement of ecosystems with the 5–10% surviving species giving rise to the Mesozoic fauna. Despite a long history of systematic studies on Permian-Triassic foraminifera, there have been few investigations into spatial and temporal patterns of survivorship and evolution during this critical interval. We interrogate a high-resolution data set comprising newly obtained and previously published foraminiferal data (including 13,422 specimens in 173 species in 62 genera) from seven well-studied Permian-Triassic successions that record a transect of platform to basin facies in South China. Shallow-water settings seen at the Cili and Dajiang sections suffered a single-pulse, sudden extinction with high extinction rates at the end of the *Palaeofusulina sinensis* Zone; deeper-water and slope environments seen at Liangfengya and Meishan experienced a two-pulse extinction in the *Clarkina yini* and *Isarcicella staeschei* zones; basinal settings, seen at Shangsi, Gujiao and Sidazhai, record a single, less devastating extinction pulse in and slightly above the *C. yini* Zone. In the Late Permian, foraminiferal diversity was greatest on the shallow platforms, where 76.4% of species recorded in our study lived. The two pulses of the Permian-Triassic extinction prompted this foraminiferal diversity hotspot to move to deeper slope settings (comprising 75.6% of contemporary species) and finally basinal settings (comprising 88.8% of species). We propose that foraminifera migrated to deeper water to avoid overheating and toxicity in shallow waters that were driven by the emplacement of the Siberian Traps and coeval volcanic activities around the Paleotethys Ocean. This study provides a methodological framework for investigating survival mechanisms for foraminifers and other taxonomic groups during mass extinction events.

## 1. Introduction

It is estimated that four billion species have existed throughout Earth history and that 99% of these are extinct (Novacek, 2001). Species naturally evolve and disappear, but the evolutionary balance of the planet has also been interrupted by several major biotic crises (McGhee et al., 2013). The well-known "Big Five" mass extinctions, and numerous lesser calamities, have pruned the branches of the tree of life over time, enabling the survivors of these events and their descendants to establish new branches and shape life on Earth as we know it. Thus, extinction survivors have played a fundamental role in the origins and macroevolution of our biosphere. A key question remains: how and why could survivors survive mass extinctions? A variety of survival strategies have been postulated for terrestrial animals, including poleward migration during times of warming (Sun et al., 2012; Benton, 2018) and an ability to burrow (Waldrop, 1988; Robertson et al., 2004). Thus, many mammalian survivors of the Cretaceous-Paleogene extinction are thought to have found refuge in underground burrows, while non-avian dinosaurs (that could not burrow) suffered major losses (Waldrop, 1988; Robertson et al., 2004). Fossil records show that tetrapods moved 10–15° poleward during the Permian-Triassic extinction, probably in response to overheating in equatorial regions (Sun et al., 2012; Benton, 2018). Survival strategies in marine organisms are poorly understood, partly because of the difficulty in evaluating detailed biological and ecological processes at the required spatial and temporal resolution through geologically brief mass extinction period intervals.

The Permian-Triassic mass extinction (PTME) was the most devastating and ecologically severe of the "Big Five" extinctions (Alroy et al., 2008; Song et al., 2018), wiping out > 90% of marine species (Erwin, 1994; Song et al., 2013) and resulting in the complete restructuring of

* Corresponding author.
*E-mail address:* haijunsong@cug.edu.cn (H. Song).

https://doi.org/10.1016/j.earscirev.2020.103329
Received 15 February 2020; Received in revised form 8 August 2020; Accepted 18 August 2020
Available online 21 August 2020

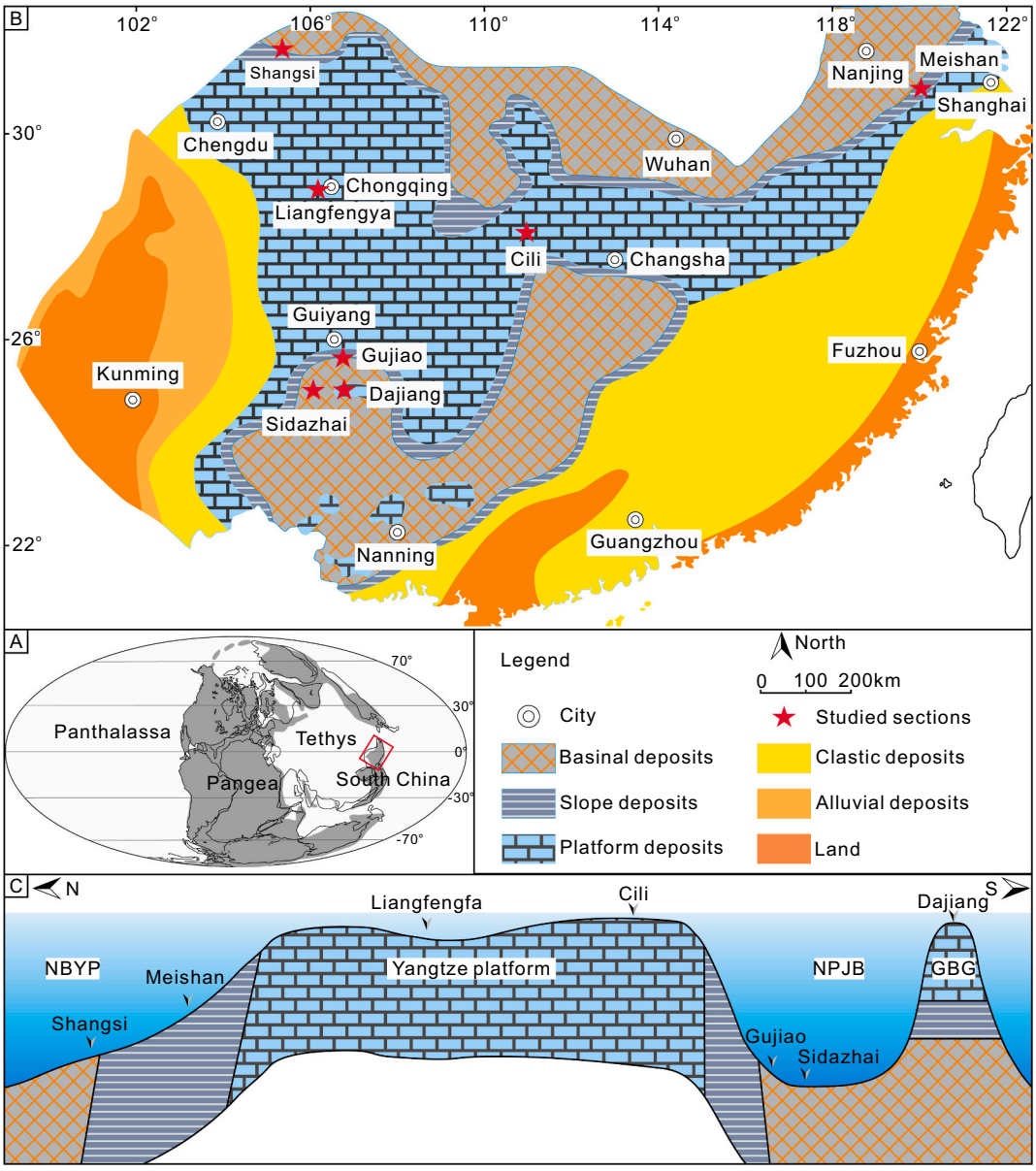


**Fig. 1.** Palaeogeographic map for the Permian-Triassic boundary interval. (A) Locations of studied sections in South China, modified from Feng (1997), Lehrmann et al. (1998) and He et al. (2013). (B) Global map modified from Scotese (2001). (C) Schematic cross-section of the South China Block in the Permian-Triassic boundary interval showing the relative water depths of our seven study sections. Red stars show the locations of study sections. Abbreviations: NBYP = Northern Basin of the Yangtze Platform; NPJB = Nanpanjiang Basin; GBG = Great Bank of Guizhou. (For interpretation of the references to color in this figure legend, the reader is referred to the web version of this article.)

life from Palaeozoic- to Mesozoic-faunas (Sepkoski, 1981). The drivers of this mass extinction have been debated for half a century, and most extinction scenarios invoke multiple climatic and environmental factors linked to the Siberian Traps large igneous province (Renne and Basu, 1995; Burgess et al., 2017; Shen et al., 2019; Chu et al., 2020) and coeval volcanic activity around the Paleotethys Ocean (Yin and Song, 2013). Volcanically-derived stress factors include global warming (Joachimski et al., 2012; Sun et al., 2012; MacLeod et al., 2017), anoxia (Isozaki, 1997; Grice et al., 2005; Bond and Wignall, 2010; Shen et al., 2016) and ocean acidification (Payne et al., 2010; Hinojosa et al., 2012; Clarkson et al., 2015).

The PTME was highly selective (Knoll et al., 1996; McKinney, 1997; Clapham and Payne, 2011; Song et al., 2013). Marine ecosystems shifted from dominance by non-motile animals to dominance by nektonic organisms (Song et al., 2018), and non-motile animals suffered higher extinction magnitudes. Extinction patterns and magnitudes among benthic organisms varied between shallow- and deep-water settings: extinctions amongst foraminifers occur as a single pulse in platform sections (Groves et al., 2005; Song et al., 2009b; Yang et al., 2016), but this group also suffered a second extinction pulse in slope settings (Song et al., 2009a). In contrast, ostracods exhibit two extinction pulses in shallow settings, and while abundant ostracods are found within the well-known Permian-Triassic microbialite unit, they disappear along with this facies in the Griesbachian substage (lower Induan Stage) (Forel, 2013; Wan et al., 2019). In slope settings, ostracods record only a single extinction pulse (Crasquin et al., 2010).

In exploring how survivors survived the PTME, Foraminifera have so far not been much considered. The large fusulinacean foraminifera were among the dominant benthos in late Palaeozoic oceans until they were eliminated during the PTME (Stanley and Yang, 1994). Smaller foraminifers also suffered severe loss but a few species survived (perhaps due to their more efficient oxygen uptake) into the Triassic

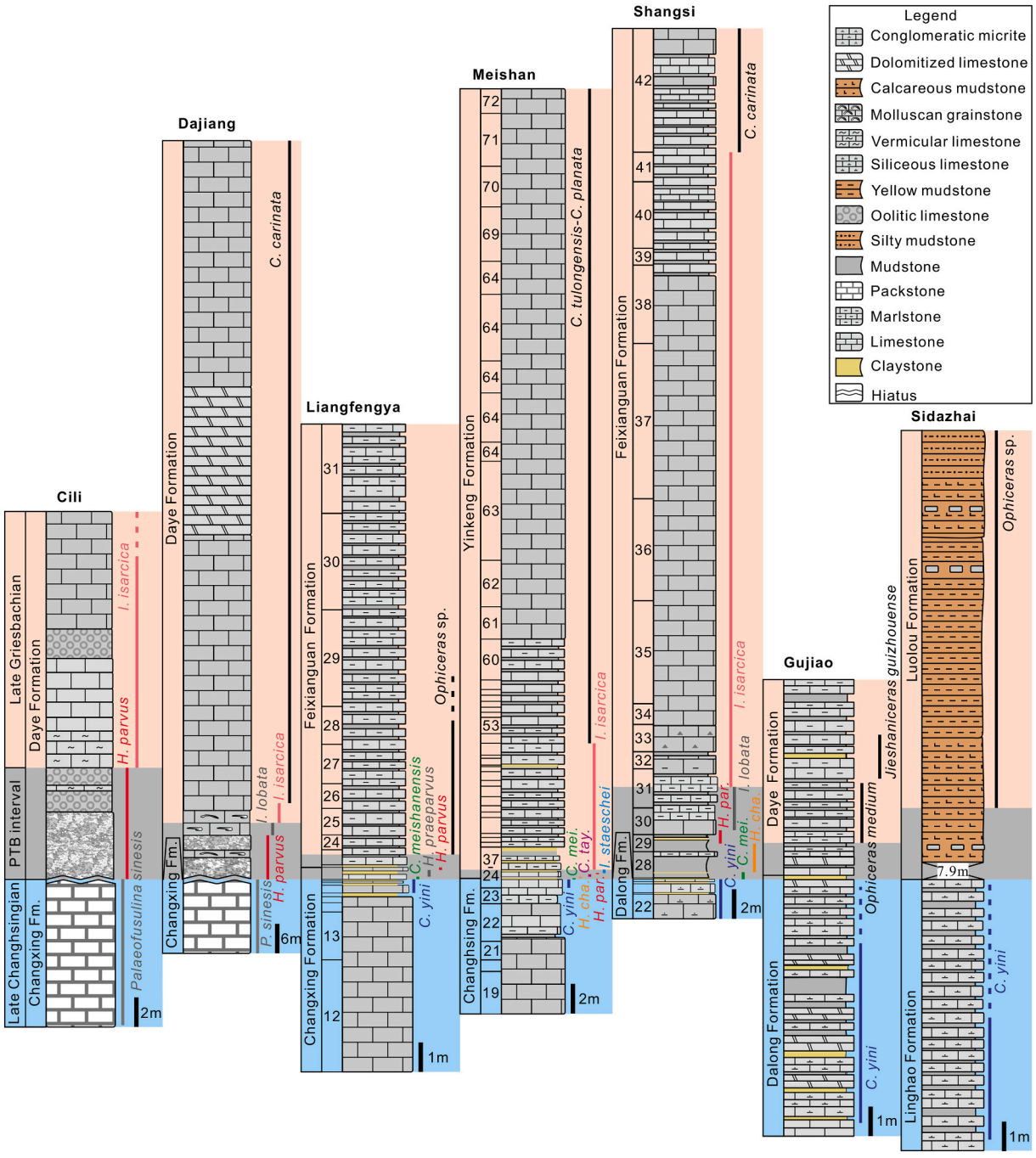


**Fig. 2.** Columnar sections of the Permian–Triassic successions at Cili, Dajiang, Liangfengya, Meishan, Shangsi, Gujiao, and Sidazhai. Biostratigraphic data of the Dajiang section from Jiang et al. (2014) and Payne et al. (2004), the Cili section from Wang et al. (2016), the Liangfengya section from Yuan and Shen (2011) and Wu (1988), the Meishan section from Yin et al. (2001), and Jiang et al. (2007), the Shangsi section from Jiang et al. (2011), Yuan et al. (2019), and Lai et al. (1996), the Gujiao section from Dai et al. (2018a) and unpublished data, and the Sidazhai section from Huang (2014) and Ji (2012) are followed herein. The blue box represents the late Changhsingian; the grey box represents the PTB interval; the pink box represents the late Griesbachian. Abbreviations: *C. yini* = *Clarkina yini*; *C. mei.* = *C. meishanensis*; *H. cha.* = *Hindeodus changxingensis*; *C. tay.* = *C. taylorae*; *H. par.* = *H. parvus*. *I. isarcica* = *Isarcicella isarcicai*. (For interpretation of the references to color in this figure legend, the reader is referred to the web version of this article.)

(Groves et al., 2005; Payne et al., 2011). Foraminifers represent an excellent group to study the above questions because they have a rich fossil record and they experienced the whole process of extinction, survival, and recovery during the Palaeozoic-Mesozoic transition (Song et al., 2011b). They are one of the most common fossil groups in Permian-Triassic marine strata due to their high abundance and the high preservation potential of their calcified or agglutinated tests. They are, therefore, perfectly suited for high-precision quantitative studies of the ecological strategies that facilitated survival during extinction events. Here, we use a detailed record from South China to investigate survival strategies during the PTME interval, and hence to unpick the underlying causes of the PTME.

There has been a long history of systematic studies on Permian-Triassic foraminifera from many regions, including the Alps (Vachard and Miconnet, 1989; Groves et al., 2007; Nestell et al., 2011; Kolar-Jurkovšek et al., 2013), Caucasia (Pronina, 1988; Vuks, 2000; Pronina-Nestell and Nestell, 2001; Vuks, 2007), Iran (Kobayashi and Ishii, 2003; Aghai et al., 2009; Kolodka et al., 2012; Nejad et al., 2015), Japan

(Kobayashi, 1997; Kobayashi, 2006; Kobayashi, 2012; Kobayashi, 2013), Tibet (Wang and Ueno, 2009; Wang et al., 2010; Zhang et al., 2013; Zhang et al., 2016), Turkey (Altiner, 1981; Altiner et al., 2000; Altiner and Altiner, 2010; Vachard and Moix, 2013), and South China (Gaillot et al., 2009; Song et al., 2009a; Song et al., 2011b; Song et al., 2015). Earlier investigations have revealed that foraminiferal faunas from shallow to deep settings were inconsistent in their response to the PTME (Gu et al., 2007; Song et al., 2009b; Zhang and Gu, 2015), thus it is necessary to investigate their spatial evolution.

In this paper, we examine multiple facies in multiple localities to reveal the spatial-temporal evolution of foraminifers during the PTME in South China. We perform a new quantitative analysis on seven sections that record different facies and environments of deposition in South China, each of which has been previously studied for its biostratigraphy, sedimentology, and geochemistry. This enables us to compare in detail, and for the first time, how these key organisms responded to the mass extinction crisis in different oceanic settings.

## 2. Key sections and stratigraphy

During the Permian-Triassic boundary (PTB) interval, the South China Block was located in low latitude eastern Paleotethys (Fig. 1B). The South China Block was a stable palaeogeographic unit from the Late Proterozoic to the Middle Triassic and records diverse depositional lithofacies from shallow-water carbonates to deep-water basin siliciclastics (Feng, 1997; Lehrmann et al., 1998; He et al., 2013). We have studied seven sections that can be divided into three distinct sedimentary environments: shallow platform, slope, and basin (Fig. 1A and C). Specifically, shallow platform facies are recorded at Cili and Dajiang, and in the lower part of the Liangfengya section (the Changxing Formation); slope facies are exposed at Meishan, in the upper part of the Liangfengya section (the Feixianguan Formation), and the lower part of the Shangsi section (the Dalong Formation); basinal facies are seen in the upper part of the Shangsi section (the Feixianguan Formation) and at Gujiao and Sidazhai. Each section preserves a continuous succession through the Permian-Triassic transition apart from Sidazhai where the basal 7.9 m of the Luolou Formation are covered. The sedimentary characteristics and biostratigraphic data for each section are discussed in detail below. We divided the successions into three parts, i.e. late Changhsingian (*Clarkina yini* Zone), PTB interval (*C. meishanensis* to *Isarcicella staeschei* zones), and the late Griesbachian. Strata in the PTB interval are sometimes referred to as transitional beds (Yin and Wu, 1985) or mixed fauna beds (Teichert et al., 1970; Sheng et al., 1984; Chen et al., 2005), characterized by mixed Permian-type and Triassic-type faunas.

### 2.1. Cili section

The Cili section, ~200 km west of Changsha city, Hunan Province, is located in the central part of the Upper Yangtze carbonate platform (Feng et al., 1993) (Fig. 1B). The Permian-Triassic sequence is composed of the Changxing and Daye Formations (Fig. 2). The late Changhsingian foraminifera *Palaeofusulina-Colaniella* Zone occurs in the upper part of Changxing Formation (Wang et al., 2009). The first appearance of *Hindeodus parvus* occurs at the base of the microbialite, i.e. lowest part of the Daye Formation (Wang et al., 2016), and it has been suggested that there is a hiatus between the Changxing and Daye formations (Yin et al., 2014). Wang et al. (2016) assign the beds above the microbialite to the *Isarcicella isarcica* Zone.

The Upper Permian Changxing Formation comprises 15 m of grey, thick-bedded bioclastic packstones with an abundant and diverse fossil assemblage that includes fusulinids, small foraminifers, calcareous algae, echinoderms, and *Tubiphytes* (Wang et al., 2009; Yang et al., 2013). Most of the bioclasts are well preserved, but some fusulinids, echinoderms, and *Tubiphytes* were fragmented, suggesting that they were transported from the edge of the reef area (Wang et al., 2009). The matrix is composed of micrite and rare calcisparite, suggesting shallow back reef lagoon deposition with some turbulence (Wang et al., 1997; Wang et al., 2009).

The Lower Triassic Daye Formation, consisting of microbialites, oolitic limestones, vermicular limestones, and limestones, has a sharp basal contact with the underlying bioclastic packstones. The lower part of the Daye Formation yields a few fossil groups at low diversity, e.g. small foraminifers, small molluscs, conodonts, and ostracods (Wang et al., 2009; Luo et al., 2013; Yang et al., 2013). The microbialite (Bed 2) has similar petrographic features to the calcimicrobial framestone seen at Dajiang. Beds 3 and 4 at Cili are oolitic limestone and vermicular limestone, respectively. The oolitic limestone is composed of well-preserved grains. These grains are spherical or ellipsoidal with diameters between 0.2 mm and 0.6 mm, and are surrounded by microspar and rarely, micrite (Wang et al., 2009). The development of microbialites and oolitic limestones suggests shallow platform deposition (Wang et al., 1997; Wang et al., 2009).

### 2.2. Dajiang section

The Dajiang section, ~120 km south of Guiyang city, Guizhou Province, was deposited on the Great Bank of Guizhou in the Nanpanjiang Basin, South China Block during the Late Permian period (Lehrmann et al., 2003; Collin et al., 2009) (Fig. 1B). Its Permian-Triassic sequence consists of the Wujiaping and Daye formations (Fig. 2). The late Changhsingian conodont *Clarkina changxingensis* is known from the upper part of the Wujiaping Formation (Lehrmann et al., 2003). The first occurrence of the basal Triassic marker, *Hindeodus parvus* is in the skeletal limestone that fills in hollows between the topmost Changxing Formation and lowermost Daye Formation (Jiang et al., 2014). Accordingly, the microbialite is also assigned to the *H. parvus* Zone (Lehrmann et al., 2003). The *Isarcicella lobata* and *Isarcicella isarcica* zones have been identified in the overlying molluscan grainstone and limestones, respectively (Payne et al., 2004; Jiang et al., 2014).

The Upper Permian Wujiaping Formation comprises 15 m of thick-bedded cherty skeletal packstone, yielding diverse and abundant fossils, including fusulinids, sponges, rugose corals, crinoids, echinoid spines, *Tubiphytes*, bivalves, gastropods and dasycladacean algae (Lehrmann et al., 2003; Song et al., 2009b). The skeletal packstone contains abundant small fossil fragments whose cavities are filled with lime-mud, suggesting deposition in a shallow platform environment near fair-weather wave base (Lehrmann et al., 2003).

The overlying Early Triassic Daye Formation comprises 16 m of massive-bedded calcimicrobial framestone interbedded with molluscan lime grainstone, yielding only a few fossils, such as pectinacean bivalves, small gastropods, small foraminifera, ostracods, rare echinoderms and brachiopods (Lehrmann, 1999; Lehrmann et al., 2003; Yang et al., 2011; Forel, 2012). The microbial fossils of the framework comprise equant to lunate globular fossils with micrite walls that form irregular, tufted, and dendritic aggregates (Lehrmann et al., 2003; Liu et al., 2007). The irregular intraframework cavities are several centimetres thick and filled with micritie and other fossil fragments (Lehrmann et al., 2003; Lehrmann et al., 2015). These microbial blooms and interlayered molluscan grainstones are characteristic of shallow marine subtidal environments (Osleger and Read, 1991; Lehrmann, 1999; Lehrmann et al., 2003).

### 2.3. Liangfengya section

The Liangfengya section, ~13 km west of Chongqing city, was deposited in the west of the Upper Yangtze platform during the Permian-Triassic transition (Fig. 1B). This section comprises the Changxing and Feixianguan formations (Fig. 2). The late Changhsingian conodont *Clarkina changxingensis* was found in the upper part of the Changxing Formation (Yuan and Shen, 2011). The Permian-Triassic boundary is

characterized by the first occurrence of *Hindeodus parvus* within a limestone (Bed 21c) in the uppermost Changxing Formation (Peng and Tong, 1999; Yuan and Shen, 2011). The beginning of the late Griesbachian is marked by the first occurrence of the ammonoid *Ophiceras* sp. (Wu, 1988).

The Upper Permian Changxing Formation (Beds 11–21) consists of 9.45 m of thick- to medium-bedded bioclastic packstones with diverse fossils, including rugose corals, brachiopods, small foraminifers, fusulinids, ostracods, calcareous algae, and conodonts (Yang et al., 1987; Tong and Kuang, 1990; Song et al., 2011a). These abundant, well-preserved fossils are contained within micrite cements (some bioclasts are micritised and abraded), suggesting that these sediments were deposited in an open platform (inter-reef) setting with occasional perturbation (Tong and Kuang, 1990; Wignall and Hallam, 1996). The packstones are interlayered with thin beds of clay that are up to a few centimeteres thick and consist entirely of illite and montmorillonite (Wignall and Hallam, 1996).

The lower part of the Feixianguan Formation is characterized by thin- to medium-bedded marl interbedded with black shale and yellowish clay (Bed 22). Bed 23 is characterized by alternations of yellow-green laminar mudstone and calcareous mudstone, yielding a few bivalves, ammonoids, and brachiopods, e.g. *Claraia grissbachi*, *C. hunanica*, and *Lingula* sp. (Yang et al., 1987). The marl is poorly bioturbated, limited to small-sized burrows, and the abundance of small pyrite framboids in beds 16–22 suggests oxygen-restricted conditions (Wignall and Hallam, 1996).

### 2.4. Meishan section

The Meishan section is located in Changxing County, Zhejiang Province (Fig. 1B), and is well known as the Global Stratotype Section and Point (GSSP) for the Permian-Triassic boundary (Yin et al., 2001). The Late Permian to Early Triassic succession is recorded by the Changxing and Yinkeng formations (Fig. 2). The conodont biostratigraphy is well established (Yin et al., 2001; Jiang et al., 2007).

The upper Changxing Formation (Beds 19–24) is composed of 11.3 m of thick- to thin-bedded bioclastic micrite and siliceous micrite, yielding diverse fossils, including foraminifers, sponge spicules, crinoids, echinoids, brachiopods, bivalves, ostracods, microproblematica, and sporadically radiolarians (He et al., 2005; Song et al., 2009a; Chen et al., 2015). Lithofacies and fossils indicate deposition in a low-energy open slope environment still within the euphotic zone (Zhang et al., 1996; Cao and Zheng, 2007; Chen et al., 2015).

The lowest part of the Yinkeng Formation is composed of marl and mudstone, interbedded with clays with planar, fine lamination. The marls are mostly composed of micrite matrix with rare fragments of foraminifers, ostracods, echinoids and brachiopods (Cao and Zheng, 2009; Chen et al., 2015). The lower part of the Yinkeng Formation records a transgressive systems tract deposited beneath storm wave base (Zhang et al., 1996). The middle to upper part of the Yinkeng Formation has been interpreted as having been deposited in a relatively deep, offshore location (Chen et al., 2007; Chen et al., 2015). Pyrite framboid and geochemical data suggest that depositional redox conditions became euxinic to dysoxic in the latest Changhsingian (Beds 25-26a), and these persisted into the basal Triassic (Shen et al., 2011; Song et al., 2012; Chen et al., 2015).

### 2.5. Shangsi section

The Shangsi section, ~230 km south of Chengdu city, Sichuan Province, was located in the Northern Basin of the Yangtze Platform during the Permian-Triassic transition (Fig. 1A), and exposes the Dalong and Feixianguan formations (Fig. 2). The biostratigraphic and cyclostratigraphic framework has been studied in detail (Lai et al., 1996; Jiang et al., 2011; Wu et al., 2013; Yuan et al., 2019).

The upper part of the Dalong Formation comprises 2.98 m of thin-bedded dark grey, organic-rich micrite, interbedded with claystone, yielding a deep-water fauna of ammonoids, radiolarians, conodonts, and small foraminifers (Li et al., 1986; Wignall et al., 1995). Both the lithofacies and fossil groups suggest deposition in an outer ramp to basinal facies (Jin, 1987; Wignall et al., 1995), somewhat deeper than Meishan.

The lowest part of the Feixianguan Formation (Bed 29) is composed of mudstone, marl, and claystone with horizontal bedding, and includes sparse conodonts, bivalves, echinoids, and foraminifers. The remainder of the lower Feixianguan Formation comprises thin- to thick-bedded marls and limestones interbedded with mudstone, and contains rare Triassic fossils. The limestone is dominated by horizontal bedding and sporadic cross bedding throughout the lower Feixianguan Formation, which suggests deposition within the reach of storm waves in a lower carbonate ramp setting (Wignall et al., 1995; Xie et al., 2017).

### 2.6. Gujiao section

The Gujiao section, ~20 km southeast of Guiyang city, Guizhou Province, was located at the northern margin of the Nanpanjiang Basin during the Permian-Triassic transition (Fig. 1B). The PTB sequence comprises the Dalong and Daye Formations (Fig. 2), which are well exposed in this area. In our study, the late Changhsingian index fossils *Pseudotirolites* sp. and *C. yini* were found in the lower part of the Dalong Formation (Miao et al., 2019). The Permian-Triassic boundary marker, *H. parvus* occurs in the basal part of the Daye Formation. The first occurrence of the Griesbachian ammonoid *Ophiceras medium* is in the uppermost part of the Dalong Formation (Dai et al., 2018a; Dai et al., 2018b). We consider that the interval from the top of the siliceous micrite to the first occurrence of *Ophiceras medium* constitutes the Permian Triassic transitional beds.

The Dalong Formation comprises 11 m of thin-bedded micrite, siliceous micrite, dolomitized limestone, and marl, interbedded with mudstone and claystone. These beds yield diverse ammonoids, nautiloids, radiolarians, small foraminifers, sponge spicules, as well as transported brachiopods and bivalves (Zheng, 1981; Feng and Gu, 2002). The siliceous micrite is characterized by spherical or elliptical radiolarian fragments surrounded by micrite, suggesting deposition in a basinal setting. The relative water depth of Gujiao is inferred to have been deeper than at Shangsi based on the abundant open marine fossils and development of anoxic conditions.

The lower Daye Formation consists of 6.6 m of thin-bedded marl and limestone interbedded with black shale and mudstone. The marl contains a low abundance fossil assemblage of ammonoids, bivalves, brachiopods, gastropods, foraminifers and ostracods (Dai et al., 2018a; Dai et al., 2018b).

### 2.7. Sidazhai section

The Sidazhai section, ~130 km south of Guiyang city, Guizhou Province, was located in the north of the Nanpanjiang Basin during the Permian-Triassic transition (Fig. 1B). The Late Permian to Early Triassic succession comprises the Linghao and Luolou Formations (Fig. 2). The conodont *Clarkina yini* has been recovered from the base of the Linghao Formation (Ji, 2012), indicating a late Changhsingian age. The lower part of the Luolou Formation yields ammonoids belonging to the *Ophiceras-Lytopiceras* assemblage (Huang, 2014), suggesting a late Griesbachian age.

The Linghao Formation comprises 13.4 m of medium- to thin-bedded limestone and siliceous limestone interbedded with siliceous mudstone and yellow mudstone, yielding well-preserved fossils, including foraminifers, radiolarians, ammonoids, brachiopods, bivalves, and conodonts (Ji, 2012; Huang, 2014). The limestone (Bed 1) consists of a 4 m thick, grey, medium-bedded limestone with chert nodules and contains pyrite framboids and diverse autochthonous fossil groups. The siliceous limestone (Bed 2) is characterized by planar lamination,

micrite fills with minor amounts of quartz, and deep-water fossil groups dominated by radiolarians, e.g. *Latentifistula* sp., *Ormistonella* sp., and *Follicucullus* sp. (Feng et al., 2000; Gao et al., 2001), sponge spicules, and small foraminifers. These sediments record deposition in a basinal setting. The depth of Sidazhai is similar to that of Gujiao, but the former is more distal from the Yangtze platform.

The lower part of the Luolou Formation comprises 14.6 m of thin-bedded lutescent calcareous mudstone interbedded with nodular limestones that yield a few bivalves, ammonoids, conodonts, and small foraminifers, e.g. *Claraia griesbachi*, *Claraia orbicularis*, *Ophiceras* sp., and *Lytophiceras* sp. (Ji, 2012; Huang, 2014; Huang et al., 2018).

## 3. Materials and methods

We analyzed 13,422 individual foraminiferal specimens observed in 981 standard thin sections ($2.2 \times 2.2$ cm$^2$) from seven Permian-Triassic transitional sections in South China. Our new data from the Liangfengya, Cili, Gujiao, Shangsi, and Sidazhai sections (see details in the Supplementary data) is supported by data from previously published records from Dajiang (Song et al., 2009b; Payne et al., 2011) and Meishan (Song et al., 2009a). We construct a temporal framework for these sections using high-resolution biostratigraphic correlations based on larger fusulinaceans, conodonts, and ammonoids. All newly obtained samples are deposited in the School of Earth Sciences, China University of Geosciences, Wuhan, China.

### 3.1. Cluster analysis

Q-mode cluster analysis was performed using the paired group algorithm with the Euclidean distance (or similarity) index (Parker and Arnold, 2003; Hammer and Harper, 2006; Schröder-Adams et al., 2008) to examine the similarities of foraminiferal assemblages in our seven sections during the Late Permian-Early Triassic interval. Our database comprises taxa at generic level and their relative abundances (as percentages) in each section and each interval. We included 63, 23, and 21 genera for the late Changhsingian (*C. yini* Zone), PTB interval, and the late Griesbachian intervals respectively. The cluster analyses were performed with PAleontological STatistics (PAST), Version 3.16 (Hammer et al., 2017), using the unweighted paired group method of arithmetic means with Euclidean similarity index to calculate the cluster trees. Foraminiferal faunas with high similarity are aggregated on one tree primarily, with smaller distances between these.

### 3.2. Confidence interval for estimating the extinction position

The "last occurrences" of fossil taxa do not necessarily represent their true extinctions because of the Signor-Lipps effect (Meldahl, 1990; Rampino and Adler, 1998). This is especially the case for those species that have less than 15% stratigraphic abundance (i.e. occurring in less than 15% of the sample intervals). Statistical analyses can generate confidence levels (such as 50% or 95%; here we employ the 50% confidence level) for the end of the stratigraphic range of a taxon. Confidence interval size depends inversely on the sampling rate, based on the length of the stratigraphic range and the number of included fossil horizons. The 50% confidence interval, calculated from the binomial distribution (Marshall, 1990; Marshall and Ward, 1996) and other improved methods (Wang and Marshall, 2004; Wang and Everson, 2007) can predict the position of the true extinction horizon with some certainty, and so we employ the 50% confidence interval method for our four platform and slope sections. The confidence interval (r) is calculated according to Strauss and Sadler (1989):

$$r = R[(1 - C)^{-1/(H-1)} - 1]$$

where C is confidence level, which in this case equals 50%, H is the number of fossil horizons, and R is the observed stratigraphic range.

### 3.3. Meldahl's method for testing the extinction pattern

Meldahl (1990) developed a method with a "stratigraphic abundance vs. last occurrence" plot to negate the Signor-Lipps effect, and test extinction patterns in the geological record. By modelling a sudden extinction of a modern molluscan biota from the tidal zone in the northern Gulf of California, Meldahl (1990) identified three extinction patterns, i.e. sudden, stepwise, and gradual. Sudden extinction exhibits an accelerated diversity decline towards the extinction horizon. Stepwise extinction demonstrates a stepped diversity decline. Gradual extinction appears as a constant decline (Meldahl, 1990, Figs. 4–6). Extinction horizons for individual species are accurately recorded when their stratigraphic abundance is higher than 15%. Meldahl's (1990) method has been applied frequently to test extinction patterns based on stratigraphic ranges in the marine fossil record (Jin et al., 2000; Groves et al., 2005; Song et al., 2009b; Angiolini et al., 2010; Jia and Song, 2018). We employ Meldahl's (1990) method for our four platform and slope sections.

### 3.4. Rarefaction analysis

Sample- or individual-based rarefaction (species accumulation curve) is an interpolation method to estimate how many species would be observed for any smaller or larger number of samples or individuals (Raup, 1975). Our sample-based rarefaction follows the methods of Colwell et al. (2004), and individual-based rarefaction follows the methods of Colwell et al. (2012). Rarefaction analyses were performed using PAleontological STatistics (PAST), Version 3.16 (Hammer et al., 2017). For sample-based rarefaction, 739 samples were analyzed. Among these, the late Changhsingian data set includes 103 platform, 74 slope, and 55 basin samples; the PTB interval data includes 118 platform, 88 slope, and 50 basin samples; the late Griesbachian data includes 45 platform, 94 slope, and 112 basin samples.

## 4. Results

Here, the systematic classification of the Order Lagenida follows Groves et al. (2003), while for other orders we follow Loeblich and Tappan (1988) and Loeblich and Tappan (1992). In total, 173 species in 62 genera (plus additional unidentified elements, Table 1) belonging to five orders (Fusulinida, Lagenida, Miliolida, Textulariida, and Involutinida) have been identified from the upper Changhsingian stage (*C. yini* Zone) of the Late Permian and Griesbachian substage of the Early Triassic. These taxa are all characteristic of the Late Permian to Early Triassic Paleotethys marine realm.

### 4.1. Cili section

We identified 1,511 specimens from 36 samples in the upper Changxing Formation. Seventy-two species belonging to 34 genera (Fig. 3) are present in the *Palaeofusulina sinensis* fusulinacean Zone–this is an index fossil zone for the late Changhsingian in South China (Zhang and Yue, 2017). Four species were identified from 54 specimens in 38 samples from the *H. parvus* Zone. The fusulinacean assemblage comprises 238 specimens in 12 species of 4 genera (Table 1). A total of 326 specimens in 17 species of 10 genera are non-fusulinacean fusulinids. The Order Lagenida is represented by 604 specimens in 32 species of 14 genera. The most abundant genera are *Pachyphloia*, *Colaniella*, *and Nodosinelloide*. The Order Miliolida includes 326 specimens in 10 species of 5 genera, dominated by *Glomomidiellopsis*, *Hemigordius*, and *Glomomidiella*. The textulariid *Ammodiscus* sp. is rarely observed in the upper Changxing Formation. During the extinction pulse, all fusulinacean genera disappeared at the bioclastic packstone/microbialite boundary. The non-fusulinacean fusulinids, *Diplosphaerina inaequalis*, and *Globivalvulina bulloides* occurred at the base of the microbialite unit but then also vanished. *Postcladella kahlori* and *Earlandia* spp. are

**Table 1**
Species diversity distribution of the main foraminifer groups in each section in the *C. yini* Zone, PTB interval, and late Griesbachian.

| Age | Order | Cili | Dajiang | Liangfengya | Meishan | Shangsi | Gujiao | Sidazhai |
|---|---|---|---|---|---|---|---|---|
| Late Griesbachian | Fusulinda | 0 | 1 | 1 | 1 | 1 | 2 | 1 |
| | Lagenida | 0 | 1 | 1 | 2 | 8 | 8 | 7 |
| | Miliolida | 0 | 1 | 0 | 0 | 1 | 2 | 0 |
| | Textulariida | 0 | 0 | 0 | 2 | 2 | 1 | 1 |
| PTB interval | Fusulinda | 3 | 2 | 1 | 4 | 3 | 0 | 0 |
| | Lagenida | 0 | 1 | 15 | 15 | 10 | 1 | 0 |
| | Miliolida | 1 | 2 | 0 | 2 | 3 | 0 | 0 |
| | Textulariida | 0 | 0 | 0 | 2 | 2 | 0 | 0 |
| *C. yini* Zone | Fusulinda | 29 | 26 | 15 | 13 | 3 | 1 | 2 |
| | Lagenida | 32 | 24 | 22 | 24 | 14 | 10 | 14 |
| | Miliolida | 10 | 7 | 2 | 9 | 8 | 2 | 2 |
| | Textulariida | 1 | 2 | 0 | 2 | 1 | 0 | 2 |
| | Involutinida | 0 | 1 | 0 | 0 | 0 | 1 | 0 |

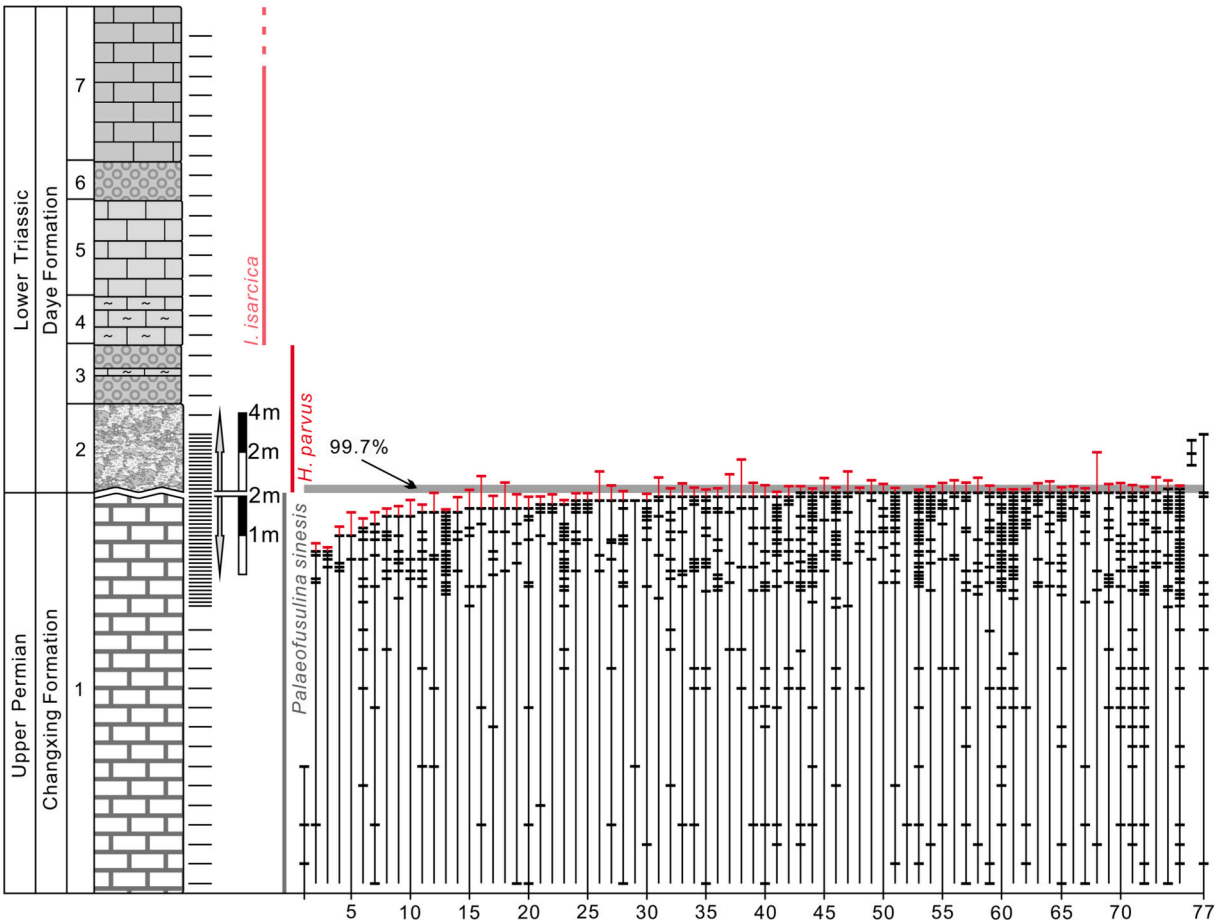


**Fig. 3.** Stratigraphic occurrences of foraminifers in the Cili section. The red lines represent 50% confidence intervals of each species. Contours indicating the predicted position of the extinction horizon are shown in grey bars. The horizontal black lines to the right of the lithologic column represent the sampling position. A list of foraminifers identified from Cili is provided as a Supplementary Table. (For interpretation of the references to color in this figure legend, the reader is referred to the web version of this article.)

documented in younger strata.

### 4.2. Dajiang section

Here we analyze the original foraminiferal data collected by Song et al., 2009b. A total of 615 specimens belonging to 60 species in 37 genera were determined from 34 thin sections from the late Changhsingian *Palaeofusulina sinensis* foraminiferal Zone at Dajiang (Table 1). Five species of five genera occur in the microbialite (in 37 samples). Three species were identified in the Griesbachian. The stratigraphic ranges of these foraminifers are shown in Fig. 3 of Song et al. (2009b). Among these, the fusulinaceans comprise 64 specimens in 7 species. Non-fusulinacean fusulinids are abundant and consist of 236 specimens in 19 species and 13 genera. The Order Lagenida is represented by 176 specimens in 24 species and 12 genera. The Order Miliolida is composed of 128 specimens in 7 species of 4 genera, of which *Glomomidiellopsis tieni* (Song et al. (2009b) reported as *Glomomidiella nestellorum*) and *Hemigordius* are the dominant taxa. The Order Textulariida has the lowest abundance and diversity with only *Ammodiscus* sp. and *Glomospira* spp. observed in the Changxing Formation. The Order Involutinida includes *Pseudovidalina* sp. with one specimen and *Globivalvulina bulloides* and *Hemigordius longus* across the skeletal packstone-calcimicrobial framestone boundary, which appear in the basal part of the microbialite, but disappear quickly. Three species, *Postcladella kalhori*, *Earlandia* spp., and *Nodosaria expolita*, appear in the microbialite - gradually at first, before the first two species become extraordinarily abundant in the earliest Triassic.

### 4.3. Liangfengya section

Thirty-four thin sections were examined from the *C. yini* Zone at Liangfengya, yielding 39 species in 21 genera (Fig. 4) amongst 279 specimens. A total of 418 specimens belonging to 16 species in 8 genera were determined from 18 thin sections from the PTB interval (Table 1). Two species with 18 specimens were collected from 18 samples in the *Ophiceras* sp. bed. The foraminiferal assemblage includes diverse lagenides, which comprise 111 specimens in 22 species of 11 genera. The Order Fusulinida includes 165 specimens in 15 species of 8 genera. Of these, the fusulinaceans comprise 140 specimens in 10 species of 4 genera. Non-fusulinacean fusulinids comprise 26 specimens in 5 species of 5 genera. *Glomomidiella nestellorum* is the only representative of the Order Miliolida. After the first extinction pulse, 16 species survived the PTB interval. The lagenides dominate this assemblage with 15 species. *Earlandia* spp. reaches extremely high abundances in the limestone. Only *Nodosaria elabugae* and *Earlandia* spp. are recorded in the late Griesbachian substage.

### 4.4. Meishan section

A total of 529 specimens from 47 thin sections have been identified from the *C. yini* Zone. The foraminiferal assemblage includes 48 species in 28 genera (see Fig. 2 from Song et al. (2009a). A total of 80 specimens belonging to 23 species in 16 genera (excluding an additional 12 unidentified species) were determined from 70 thin sections from the PTB interval. Five species with 178 specimens were identified from 39 samples in the late Griesbachian. Among these, 201 specimens in 24 species of 12 genera belong to Lagenida. The fusulinaceans are represented only by *Reichelina* spp. The non-fusulinacean fusulinids include 181 specimens in 11 species of 12 genera. The Order Miliolida is represented by *Hemigordius* and *Multidiscus* with ten species between them. The Order Textulariida includes *Ammovertella inversus* and *Pseudoammodiscus parvus*. Lagenides become more dominant following the latest Permian extinction (including eleven indeterminate species). *Tuberitina* sp. are the only representatives of the Order Fusulinida. *Hemigordius* sp. A is also found in the PTB interval. The agglutinated tests of *Glomospira* spp. and *Ammodiscus* sp., are recorded by single specimens. Above the level of the earliest Triassic extinction, the Yinkeng Formation yields only five species. The disaster species *Earlandia* sp. appears with high abundance.

### 4.5. Shangsi section

A total of 27 thin sections were examined from the *C. yini* Zone at Shangsi, yielding 26 species in 19 genera (Fig. 5) amongst a total of 174 specimens. Eighteen species in 15 genera have been identified from the PTB interval (from 46 samples). Griesbachian strata yielded 12 species in 9 genera from 86 samples. In the *C. yini* Zone, 65 specimens in 14 species of 10 genera belong to Lagenida. The Order Fusulinida is represented by 14 specimens in 3 species. The Order Miliolida includes 8 species in 5 genera. The Order Textulariida includes *Glomospira* sp. During the PTB interval, the foraminiferal assemblage is relatively diverse, and includes 18 species. Small and elongated lagenid elements dominate the assemblage. Fusulinida and Miliolida include 2 and 4 species, respectively, in the PTB interval. Agglutinating foraminifera are represented by *Ammodiscus* sp. and *Glomospira* sp., and these survive into the late Griesbachian. A total of 12 species from 353 specimens were collected in late Griesbachian strata (Table 1). Lagenida is represented by 8 species. The Fusulinida and Miliolida are represented by *Earlandia* sp. and *Postcladella kahlori*, respectively.

### 4.6. Gujiao section

Data from the Gujiao section come from the analysis of 52 thin sections. A total of 43 specimens, including 13 species in 11 genera (Fig. 6) have been identified from the late Changhsingian. The Order Lagenida dominates the foraminiferal assemblage at Gujiao and is represented by 33 specimens in 10 species and 8 genera (Table 1). The Order Fusulinida is represented by *Earlandia* sp. The Order Miliolida is represented by *Glomomidiella* sp. The Order Involutinida includes *Pseudovidalina* sp. Three specimens belonging to *Nodosinelloides* spp. are documented from the PTB interval. Foraminifers rebound in late Griesbachian strata and 149 specimens have been obtained from 19 thin sections. These belong to 11 species in 11 genera (plus one additional indeterminate genus and species A). The Lagenida become increasingly dominant both in abundance and taxonomic richness. The miliolids are represented only by *Planiinvoluta* sp. and *Glomomidiella* sp. The Order Fusulindia is represented by *Earlandia* sp. and *Dagmarita* sp. A in the Daye Formation. The most common agglutinated test in our samples is that of *Glomospira* sp., which occurs in late Griesbachian strata.

### 4.7. Sidazhai section

A total of 143 specimens belonging to 16 species in 12 genera (Fig. 10) have been determined from 26 thin sections from the Linghao Formation. The Order Lagenida is represented by 132 specimens in 13 species of 6 genera (Table 1). The non-fusulinacean fusulinids are represented by single occurrences of *Neoendothyra parva* and *Dagmarita* sp. in the upper part of the limestone unit. Miliolida is represented by only two specimens of *Glomomidiella* sp. and *Hemigordius qinglongensis*. Textulariides, including *Ammodiscus* sp. and *Glomospira* spp. are observed. The lower part of the PTB interval in this section was covered. The upper part of the PTB interval is represented by calcareous mudstone with no foraminifera present. Foraminifers are seen again in limestones from the late Griesbachian. The assemblage is dominated by lagenides. Both *Earlandia* sp. and *Ammodiscus* sp. are represented by single specimens in the lower part of the Luolou Formation.

## 5. Late Permian-Early Triassic foraminiferal fauna

Three clusters (Fig. 8A–C) are identified from seven sections during the late Changhsingian, PTB interval, and late Griesbachian. They are

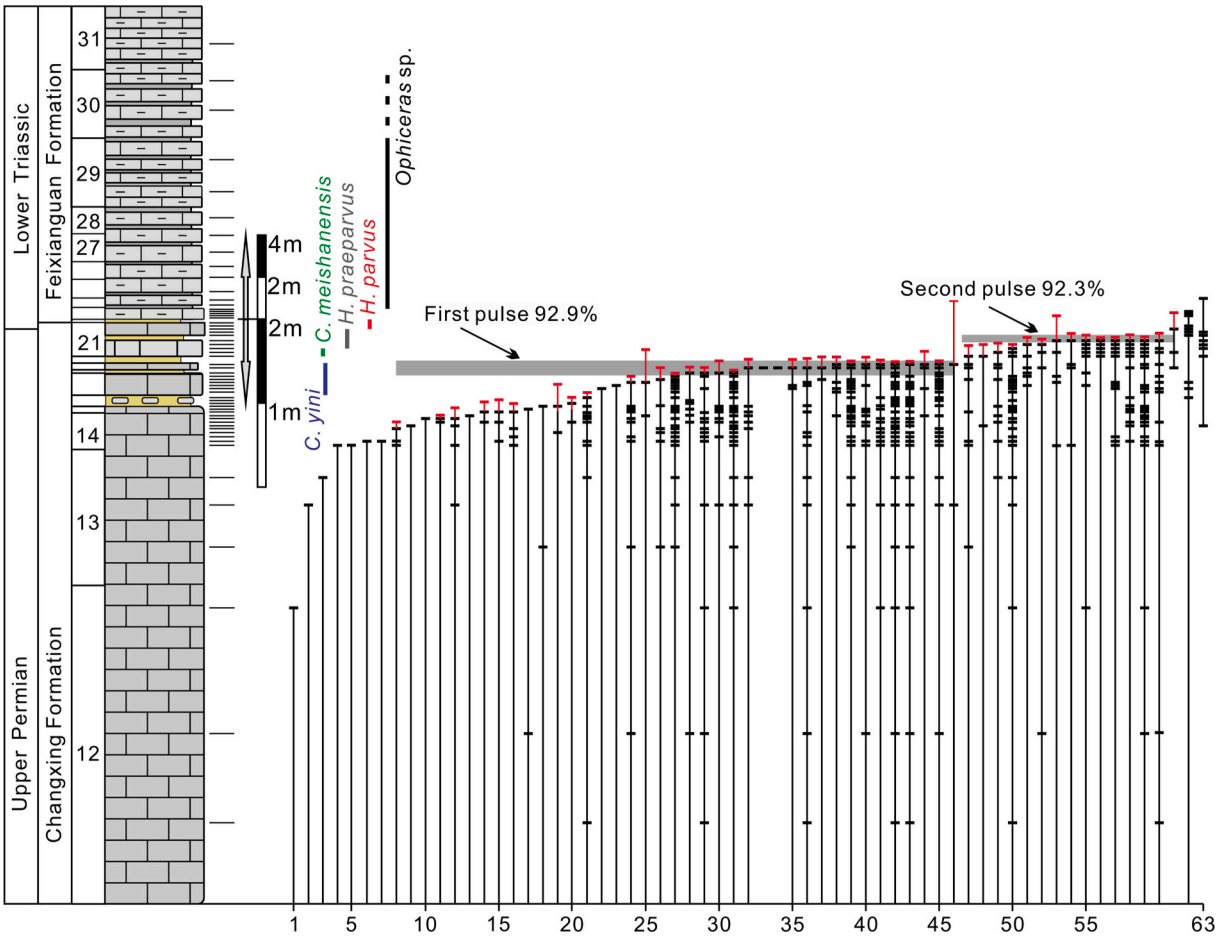


**Fig. 4.** Stratigraphic occurrences of foraminifers at the Liangfengya section. The red lines represent 50% confidence intervals of each species. Contours indicating predicted positions of the extinction horizon are shown in grey bars. A list of foraminifers identified from Liangfengya is provided as a Supplementary Table. (For interpretation of the references to color in this figure legend, the reader is referred to the web version of this article.)

named after the dominant genera and species: A1. *Palaeofusulina-Colaniella* assemblage; B1. *Hemigordius* assemblage; and C1. *Rectostipulina* assemblage in the late Changhsingian (Fig. 8A); and A2. *Postcladella kalhori* assemblage; B2. *Geinitzina* assemblage; and C2. undetermined (lack of specimens) from the PTB interval (Fig. 11B). These clusters appear to be depth-controlled, and so we name them additionally as the A-platform assemblage, B-slope assemblage, and C-basin assemblage, respectively. We did not identify the foraminiferal assemblages for the earliest Triassic due to the paucity of preserved specimens.

### 5.1. Late Changhsingian foraminiferal fauna

A total of 143 species in 56 genera were determined from the late Changhsingian (*C. yini* Zone) foraminiferal fauna. The Fusulinida dominate the platform assemblages with some larger taxa with complex morphology, and then these decrease in abundance rapidly offshore, with some small fusulinids recorded in slope areas and only a few elements found in basinal settings. The Lagenida dominate the slope and deeper assemblages and comprise small and elongated infaunal elements. Their larger and more robust representatives, such as *Pachyphloia* and *Colaniella*, preferred the shallow platform. The Miliolida is represented by a few taxa on the platform, and some generalists spread into basin assemblages, whilst the Textulariida is of low abundance and low diversity in all environments.

#### 5.1.1. Platform settings

A platform foraminiferal assemblage (the *Palaeofusulina-Colaniella* assemblage) was identified from Dajiang, Cili, and Liangfengya (Fig. 8A). A total of 110 species in 46 genera were identified. This assemblage is characterized by the frequent occurrence of shallow-water taxa such as fusulinids, large lagenids, and miliolids. Other ecological generalists occur with moderate abundance.

Large fusulinids had relatively low diversity but were still prevalent on the shallow seafloor. *Palaeofusulina* and *Reichelina* are the most abundant fusulinids in the *Palaeofusulina-Colaniella* assemblage in South China, and these taxa also flourish in other shallow platforms in the Caucasus, Thailand and Japan (Sakagami and Hatta, 1982; Pronina-Nestell and Nestell, 2001; Kobayashi, 2006). *Palaeofusulina* and *Reichelina* occur in varying quantities in platform assemblages (Fig. 9), probably having been transported (Tong and Kuang, 1990; Lehrmann et al., 2003). Other large fusulinids like *Nankinella*, *Pisolina*, *Sphaerulina*, and *Parareichelina* are rare or absent, and comprise no more than 3% (no more than three species in one section) in the platform assemblage. Fusulinaceans have a relatively large test and they demanded more food. They also had specialized microhabitats (Brasier, 1995; Beavington-Penney and Racey, 2004) that were adaptations for algal symbionts (Lee et al., 1979; Cowen, 1983; Lee and Hallock, 1987; Groves and Yue, 2009; Lee et al., 2010; Forsey, 2013) due to their wall structure, ecology, facies distribution, and their evolutionary pattern. Without exception, these taxa are mostly restricted to the shallow euphotic zone. Fusulinaceans also appear to be susceptible to extinction driven by environmental change (Stanley and Yang, 1994; Yang et al., 2004; Song et al., 2013). Shallow-water fusulinids such as *Palaeofusulina*, *Pisolina*, *Nankinella*, and *Sphaerulina* produced ovate or fusiform

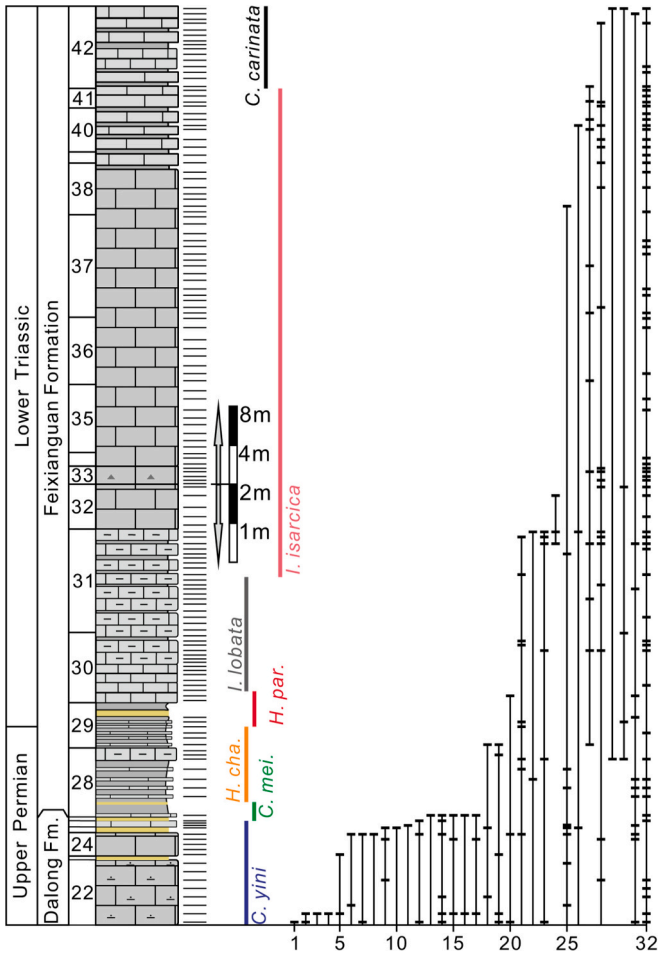


**Fig. 5.** Stratigraphic occurrences of foraminifers in the Shangsi section. A list of foraminifers identified at Shangsi is provided in a Supplementary Table.

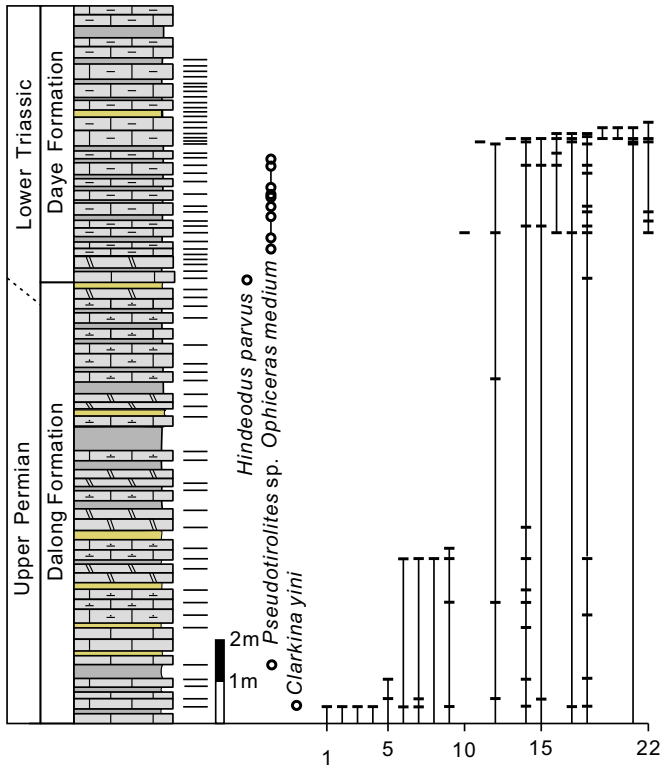


**Fig. 6.** Stratigraphic occurrences of foraminifers in the Gujiao section. A list of foraminifers identified at Gujiao is provided in a Supplementary Table.

tests with thick walls to prevent photoinhibition in bright sunlight and test damage in turbulent water (Beavington-Penney and Racey, 2004). The genus *Reichelina* occurs in relatively deeper habitats (Fig. 9), which might have been a response to competitive pressure and morphological adaptation for endosymbiont advantage (Beavington-Penney and Racey, 2004).

The non-fusulinacean fusulinids are another important component of late Changhsingian assemblages, mainly comprising members of superfamilies Biseriammininae and Palaeotextulariidae, with < 10% of occurrences in the platform assemblage. The Superfamily Palaeotextularoidea is very common in Paleotethys and eastern Panthalassa (Lin et al., 1990; Kobayashi, 2006; Gaillot and Vachard, 2007; Vachard, 2016). The Biseriammininae mainly includes *Globivalvulina*, *Dagmarita*, and *Paraglobivalvulina*, all of which preferred shallow platform settings. Of these, the small subglobular tests *Dagmarita* are most common (up to 9.43% of occurrences, Fig. 9) and with stable abundances in platform sections. *Globivalvulina* is found at moderate abundance, ranging from 0.0% (Liangfengya) to 7.8% (Dajiang) of the total, and this genus is followed by *Paraglobivalvulina* at less than 1%. The Palaeotextulariidae includes *Cribrogenerina*, *Climacammina*, *Deckerella*, and *Palaeotextularia*. *Palaeotextularia* is the most prevalent genus in platform assemblages, where it ranges from 0.26% to 5.37% of total abundance (Fig. 9). These are followed by *Cribrogenerina*, *Deckerella*, and *Climacammina*, although the abundances of these decrease to zero at Liangfengya. Our collections of Palaeotextulariidae are consistent with previous suggestions that they are mostly constrained to settings above fair-weather wave base (e.g. in the Lower Carboniferous; Gallagher, 1998). They probably had an epifaunal to shallow infaunal herbivorous lifestyle, and their strong and thick tabular tests protected them from currents (Murray, 2006). The Superfamily Endothyracea includes *Postendothyra* and *Neoendothyra*, found in higher quantities at Dajiang. However, these comprise less than 2.3% of the total taxa, and they eventually disappear at Liangfengya. The primitive and small forms, such as *Diplosphaerina* and *Earlandia* comprise low quantities but occur stably in platform sections (Fig. 9). Finally, some endemic fusulinids, such as *Sengoerina* and *Tetrataxis*, are occasionally found in shallow platform assemblages.

The large lagenids, such as *Pachyphloia* (ranging from 3.14% to 10.39% of occurrences, Fig. 9) and *Colaniella* (ranging from 0.72% to 8.07% of occurrences, Fig. 9) share a similar life strategy with the elongated non-fusulinacean fusulinids (Insalaco et al., 2006; Zhang, 2015) and they are prevalent in shallow sites, but not in deeper waters. They are characterized by thicker, stronger walls, which enable them to live in shallow, turbulent environments. The small lagenids are dominated by *Nodosinelloides*, ranging from 5.76% to 12.36% of the total in the *Palaeofusulina-Colaniella* assemblage. Some small lagenids are present at low, but steady abundances in platform sections, such as *Geinitzina*, *Frondina*, *Ichthyofrondina*, and *Robuloides* (< 4.66%, Fig. 9). Other elements, i.e. *Rectostipulina*, *Pseudolangella*, *Protonodosaria*, and *Cryptoseptida*, occur sporadically and at low diversity in platform settings.

The Order Miliolida includes many opportunists and ecological generalists that normally occur in low quantities, but proliferated rapidly when conditions were favorable (Kauffman and Harries, 1996; Groves and Altiner, 2005). During the late Changhsingian interval, the large miliolids (such as taxa from families Hemigordiopsidae and Neodiscidae) colonized and flourished in their preferred habitats on shallow carbonate platforms (Fig. 9). The dominant miliolid in very shallow sections (Dajiang and Cili) is *Glomomidiellopsis*, but it is absent at Liangfengya. *Glomomidiella* and *Hemigordius* are found at low abundances in platform assemblages (1.08–4.07%). Genera like

*Agathammina* and *Neodiscopsis* occur rather sporadically and are restricted to shallow settings (Gaillot and Vachard, 2007; Gaillot et al., 2009). Most of the miliolids in this study are coils of undivided tubular chambers and inflated to subspherical or discoid larger forms whose life strategy was most likely surficial or epifaunal (Chan et al., 2017).

In contrast to other groups described here, the Textulariida constructed agglutinated tests. The textulariides have one of the longest foraminiferal fossil records and inhabit the broadest range of habitats from coast to deep ocean. The Order Textulariida has the lowest abundance and diversity in all our assemblages. The agglutinated textulariides demonstrate ecological advantages in clastic facies (such as clastic shelf and abyssal environments) when compared to carbonate facies (Armstrong et al., 2004; Murray, 2006). Their agglutinated tests are usually poorly preserved, and are difficult to identify (Hemleben et al., 1990; Song et al., 2007). In our collections, *Glomospira* sp. and *Ammodiscus* sp. are present in platform assemblages, but none of these comprises more than 2% of individuals (Fig. 9).

#### 5.1.2. Slope settings

A slope foraminiferal assemblage (the *Hemigordius* assemblage) was identified at Meishan and Shangsi (Fig. 9). A total of 63 species in 36 genera were identified in this assemblage, which is characterized by the frequent occurrence of small lagenids, non-fusulinacean fusulinids, opportunistic miliolids, and a low abundance of agglutinated tests.

The fusulinids are represented only by *Reichelina* spp., comprising 3.78% of the assemblages, and they disappear at Shangsi. The non-fusulinacean fusulinids include 11 genera in the *Hemigordius* assemblage, but only three genera, *Dagmarita*, *Globivalvulina*, and *Diplosphaerina*, recorded at both Meishan and Shangsi (*Globivalvulina* is recorded in the PTB interval at Shangsi). The non-fusulinacean fusulinids are dominated by Biseriamininae (mainly *Dagmarita*) and *Diplosphaerina* (11.30%). The lower limit of taxa, such as *Palaeotextularia* and *Paraglobivalvulina* could not reach the depth in the Shangsi section. *Globivalvulina* and *Paraglobivalvulina* are characterized by biserial with planispiral chambers strongly enveloping a subglobular test. Their test structure suggests an epifaunal life position with mobility in turbulent eutrophic environments (Setoyama et al., 2011; Zhang, 2015). With increasing water depth, the percentage of these taxa falls, whilst the small lagenids become dominant. This pattern is also reported from other regions such as Iran, as well as other sections in South China (Insalaco et al., 2006; Gu et al., 2007; Vachard et al., 2010; Zhang and Gu, 2015). The lagenids are dominated by those with a small elongate test, such as *Nodosinelloides*, comprising 20% of the fauna, followed by *Frondina* and *Geinitzina*. The larger lagenids such as *Pachyphloia* and *Colaniella* occur at Meishan at less than 1% abundance. Other ecological generalists, such as *Cryptoseptida*, *Rectostipulina*, and *Robuloides* are found in relatively low to moderate abundances (< 4% of occurrences). The smaller discoidal test, *Hemigordius* flourishes in our slope assemblage, but rarely occurs in the other assemblages. *Glomomidiella* is also found in this assemblage with high abundance at Shangsi (Fig. 9) whilst *Multidiscus padangensis*, *Planiinvoluta* sp., and? *Meandrospira* sp. are occasionally recorded in the *Hemigordius* assemblage, at < 5.8% abundance. The textulariides are represented by *Pseudoammodiscus*, *Ammovertella*, and *Glomospira* but with low abundance and diversity.

#### 5.1.3. Basinal settings

A basin foraminiferal assemblage (the *Rectostipulina* assemblage) was identified from Gujiao and Sidazhai (Fig. 9) where a total of 29 species in 19 genera were identified. This assemblage is dominated by small, elongate and flattened Lagenida, including *Nodosinelloides*, *Protonodosaria*, *Ichthyofrondina*, and *Frondina* with total relative abundances up to 92% (at Sidazhai). The elongate tubular test *Rectostipulina* is also important in this assemblage, and its abundance increases rapidly in basinal environments to 34% on average. Most lagenids are generalists that could tolerate and spread into various environments (Murray, 2006; Gaillot and Vachard, 2007) but the small lagenids do not reach their maximum quantities within the shallow environments; instead, they are most important in basinal settings. Other groups occur at low diversity and abundance in the *Rectostipulina* assemblage. Within the Order Fusulinida, no large fusulinids occur in the basinal assemblage. The non-fusulinacean fusulinids are represented by three species with sporadic occurrences at Gujiao (including *Earlandia* sp.) and Sidazhai (including *Dagmarita* sp. and *Neoendothyra parva*). The lifestyle of *Dagmarita* might have been epifaunal because the outer margins of its chambers are joined with needle-like structures, which might have served to fasten the test to the sediment surface. Aided by their life strategy and small tests, *Dagmarita* was able to tolerate basinal environments. The lenticular and planispiral involute tests of *Robuloides* and *Neoendothyra* are not only similar to each other in morphology, but also in spatial distribution. It is possible that they both developed a flattened depressed planispiral form (with increased surface area to volume) as a strategy for living in or above shallow sediments (Setoyama et al., 2011; Chan et al., 2017). The miliolids and textulariides are sporadically observed at low diversity and abundance.

The planispiral involute test *Robuloides* occurs in low numbers in platform assemblages, reaching its greatest abundance at Liangfengya, at 8.3%. Other taxa like *Langella*, *Nodosaria*, *Pseudolangella*, and *Pseudoglandulina* (each < 1% abundance) are not strictly limited by lithofacies, but regularly occur in the platform to basinal assemblages. Finally, some endemic lagenids, like *Pseudoglandulina*, *Cryptoseptida*, *Calvezina*, and *Eocristellaria* are seen occasionally in various assemblages.

### 5.2. PTB interval foraminiferal fauna

Late Changhsingian foraminifera were major casualties of the latest Permian extinction, and the small number of survivors, augmented by a few newcomers, make up the PTB interval foraminiferal fauna (Fig. 10). A total of 41 species in 23 genera were identified from this interval, and most of the survivors are seen in slope settings. The Order Fusulinida includes five species in five genera in the microbialite and slope facies. The Lagenida, which includes 29 species, dominates the slope and basinal environments with small elongated infaunal taxa. The Miliolida is represented by five species, among which is the disaster taxon *Postcladella kalhori*, which is very abundant in the microbialite. The Textulariida is represented by *Ammodiscus* sp. and *Glomospira* sp. in slope and basinal facies.

#### 5.2.1. Platform settings

The platform *Postcladella kalhori* foraminiferal assemblage is identified at Dajiang and Cili. The eponymous species is one of the most common foraminiferal taxa to be found in the microbialite (Altiner et al., 1980; Hips and Pelikán, 2002; Groves et al., 2005; Song et al., 2016). Foraminifers from this unit are generally of low diversity and abundance, but some taxa occur sporadically at extremely high abundance –the so-called disaster taxa (Song et al., 2016) that include *Postcladella kalhori*, *Globivalvulina bulloides* and *Earlandia* spp. *Globivalvulina bulloides*, *Hemigordius longus* and *Diplosphaerina inaequalis* are found at the base of the microbialite but disappear above that level. *Nodosaria expolita* (small lagenids) are also found but with extremely low abundance and diversity in the *Postcladella kalhori* assemblage. No textulariides are found in the microbialite, which indicates that microbial blooms may have provided unsuitable habitats for agglutinated foraminifers.

#### 5.2.2. Slope settings

The slope *Geinitzina* foraminifer assemblage was identified at Liangfengya and Meishan. During the PTB interval, dominant taxa are elongate and flattened lagenid tests, with *Nodosinelloides* and *Geinitzina* as the most abundant genera, at 40.43% and 17.7% of occurrences, respectively. *Nodosaria* and *Robuloides* are found at moderate abundance in the *Geinitzina* assemblage. Other taxa, including *Amphoratheca*,

*Rectostipulina*, and *Frondina* are also rarely found in the PTB interval. The Order Fusulinida is represented by sporadically occurring *Diplosphaerina inaequalis*, *Globivalvulina bulloides*, *Neoendothyra* sp., and *Tuberitina* sp. in the PTB interval but these vanish during the earliest Triassic extinction. *Earlandia* spp. bloomed in slope settings, and this genus persists into the Triassic. *Ammodiscus* and *Glomospira* are also seen at very low abundance and diversity at Meishan.

#### 5.2.3. Basin settings

Basinal foraminiferal assemblages are recorded in the PTB interval at Shangsi and Gujiao. Shangsi has a moderately abundant foraminiferal assemblage, whilst Gujiao yields only *Nodosinelloides* spp. No foraminifera are found in this interval at Sidazhai. The assemblage at Shangsi is similar to the *Geinitzina* assemblage, but with increased dominance of lagenids and miliolids. A few Lazarus taxa, such as *Tezaquina clivuli* and *Planiinvoluta* sp. are seen at Shangsi where they occur in remarkable quantities in comparison to the late Permian fauna.

### 5.3. Late Griesbachian foraminiferal fauna

The diversity of foraminifera decreased during the earliest Triassic extinction, and 27 species in 18 genera have been determined from late Griesbachian strata, most of which are known from basin settings. The Order Fusulinida comprises two species, whilst the Lagenida includes 18 species that dominate basinal environments with their small elongated and flattened tests (Fig. 11). The Miliolida is represented by four species at low abundance. The Textulariida is represented by *Ammodiscus* sp. and *Glomospira* sp. in slope and basinal settings.

#### 5.3.1. Platform settings

Foraminifers occur in platform settings at extremely low diversity and abundance, and only three species (*Earlandia* sp., *Postcladella kalhori*, and *Nodosaria expolita*) have been observed in our study. Payne et al. (2011) reported three further species (*Postcladella grandis*,? *Hoyenella* sp., and? *Cornuspira*? *mahajeri*) in the Griesbachian substage, but the latter two had indeterminate identification and were represented by only one specimen each.

#### 5.3.2. Slope settings

Six species are found in the slope assemblage in the late Griesbachian. Of these, only *Earlandia* sp. occurs with occasional high abundance at both Liangfengya and Meishan. The lagenids are represented by *Nodosaria elabugae*, *Nodosinelloides aequiampla*, and *Lingulina* sp. with several specimens. The Order Miliolida includes *Glomospira regularis* and *Glomospira* sp. B at Meishan.

#### 5.3.3. Basin settings

The basin assemblage is more diverse than contemporaneous assemblages in shallower environments. A total of 24 species in 17 genera have been identified, including *Earlandia* sp. and *Dagmarita* sp. A. The Lagenida is represented by several relict genera (Fig. 11), such as *Nodosinelloides*, *Frondina, Rectostipulina*, and *Nodosaria* that dominate the earliest Triassic foraminiferal assemblages in abundance and diversity. These taxa are characterized by small, uniserial flattened tests, which might have benefitted from gas exchange in dysoxic to anoxic sediments due to their increased surface area to volume ratio (Kaiho, 1994). The Miliolida is sporadically represented by *Postcladella kalhori*, *Glomomidiella* sp., and *Planiinvoluta* sp. The Textulariida comprises *Glomospira* sp., *Ammodiscus* sp., which are found in low abundance.

## 6. Extinction pattern

It is well known that foraminifers suffered a catastrophic reduction in both diversity and abundance during the PTME, not only in South China but globally (Tappan and Loeblich, 1988; Tong and Shi, 2000; Groves and Altiner, 2005). The stratigraphic distributions of foraminifers from our study sections show varying patterns of decline in the run-up to the PTB (Fig. 12). Here, we explore three distinct extinction patterns in the foraminifera during the PTME.

### 6.1. Single abrupt extinction pulse with a few survivors in platform settings

The 50% confidence interval (red line, Fig. 3) method indicates a sudden extinction at Cili (a platform setting) at the base of the microbialite. Using 50% confidence intervals, we show with dark stippling (Fig. 3) in the microbialite interval that 26 species died out at the extinction horizon, and 23 species below. Calculation of the binomial distribution of these 71 taxa (excluding 1, *Glomospira* sp.; 76, *Postcladella kahlori*; 77, *Earlandia* sp. in Fig. 3) indicates with 99.7% probability that the extinction horizon lies within the dark stippled area of Fig. 3, a 19.7 cm interval around the base of the microbialite (Marshall and Ward, 1996). Further, a total of 98.6% (71/72) of species disappeared in the PTB interval. Plots from Cili exhibit hollow distribution curves consistent with a pattern of diversity decline in a simulation of sudden extinction (Meldahl (1990), and 83.3% (60/72, Fig. 12A) of species disappear in the topmost 50 cm of the packstone. The last occurrences of 31 of all 36 species (86.1%) with stratigraphic abundances > 15% disappear in the same interval. *Globivalvulina bulloides* and *Diplosphaerina inaequalis* survived the main extinction pulse, but these too eventually became extinct.

The same 50% confidence interval method also indicates that most species reach the extinction horizon at Dajiang (platform). The predicted position of the true extinction horizon lies within a 62 cm interval that includes skeletal packstone and the microbialite. Using the 50% confidence intervals method, foraminifers show 17 species endpoints below and 16 species endpoints within the 62 cm dark stippling, suggesting there was one sudden extinction, with a 97.1% probability that the extinction horizon lies within the predicted range. A total of 93.3% (56/60) of taxa became extinct at Dajiang in the late Changhsingian. Although plots of stratigraphic abundance versus last occurrence indicate that a few taxa started to disappear a few metres below the PTB, a large number of species (51.9% of taxa, or 28/54, pink boxes in Fig. 12B) disappear in the topmost 60 cm of packstone, in the latest Changhsingian. The last occurrences of 11 of all 13 species (84.6%) with stratigraphic abundances > 15% disappear in the same interval (Song et al., 2009b), which also suggests a sudden extinction. *Globivalvulina bulloides* and *Hemigordius longus* cross the packstone-microbialite boundary and appear in the basal part of the microbialite unit, but they do not reappear in younger strata (Song et al., 2009b).

To summarize, these two shallow platform sections suffered an abrupt extinction pulse (Fig. 13A), which wiped out 98.6% and 93.3% of species at Cili and Dajiang, respectively. The abrupt extinction pattern documented here has also been identified in other regions, such as Turkey (Groves et al., 2005), the southern Alps (Groves et al., 2007), and northern Iran (Angiolini et al., 2010). The latest Permian extinction pulse was so catastrophic that only six species are recorded in the microbialite unit and three of these disappeared quickly. The earliest Triassic extinction pulse did not occur in foraminifers in platform settings. The “microbialite refuge” idea (Forel, 2013; Foster et al., 2018; Foster et al., 2019) is that the shallow microbiolite environments were a shelter for some invertebrates, such as ostracods, bivalves, gastropods, and brachiopods. But data from these two sections and some unpublished data (the Jianzishan, Shanggang, and Youping sections in South China) indicate that shallow settings were unlikely to have been refuges for foraminifers.

### 6.2. Two-pulse extinction in slope settings

The grey contours in Fig. 4 indicate the predicted position of the extinction horizon, assuming a two-step decline at Liangfengya, which was located on the open platform to the upper slope (considering the water depth in the Upper Yangtze platform) when the mass extinction

occurred. The first predicted extinction interval is located in a 16.8 cm thick interval between beds 17 and 19 (*C. yini* to *C. meishanensis* zones) with 92.9% probability (Fig. 4). Foraminifers show 50% confidence intervals for ten species endpoints below and ten species endpoints within the first predicted extinction interval. Meanwhile, plots of stratigraphic abundances versus last occurrences of taxa from Liangfengya indicate a sudden decline during the first pulse that eliminated 47.7% of taxa (27/57, Fig. 12C) in bed 19 or slightly below this interval. The last occurrences of all 15 species with stratigraphic abundances > 15% are in the same interval. The second predicted extinction interval is between the top of beds 21a and 21b (7 cm interval) with 92.3% probability. The 50% confidence-interval endpoints of the foraminifers include four species below and seven species within the second contour. Fifteen out of 17 species (88.2%, pink boxes in Fig. 12C) disappear in the second extinction pulse, including all nine species with stratigraphic abundances > 15%.

Data from the Meishan section (slope) confirm the hypothesis that there were two extinction levels, in beds 25 and 28 (Song et al., 2009a, fig. 2), and this accords with stratigraphic abundance versus last occurrence data (Fig. 12D). The 50% confidence interval method predicts that the extinction interval lies in bed 25 at Meishan with 99.5% probability. The 50% confidence interval of last occurrences is bracketed by 14 species with endpoints above and 19 species with endpoints within the extinction interval. The first pulse sees 76.6% of taxa (49/64) disappear within a 10 cm stratigraphic interval (i.e. uppermost 10 cm of Bed 24e) or slightly below this interval (Song et al., 2009a) and 82.4% (14/17) of taxa with stratigraphic abundances > 15% disappear in this interval. The second predicted extinction interval lies between bed 28 and the lower part of bed 29 with 81.1% probability, with eight species having 50% confidence-interval endpoints above and seven endpoints within the secondary predicted extinction positional interval. The second pulse eliminated 94.1% of taxa (32/34) in the 10 cm stratigraphic interval (i.e. the base of Bed 28), and eight species with stratigraphic abundances > 15% disappear in this interval.

To sum up, both Liangfengya and Meishan show two extinction pulses (Fig. 13A), a pattern also seen in southern Turkey, where the first pulse occurs at the base of oolitic limestones and the second pulse at the base of a microbialite (Altiner, 2013). Liangfengya and Meishan exhibit similar extinction patterns, hinting at shared processes (discussed below), with the first pulse eliminating taxa with large, complex morphologies, and the second pulse chiefly affecting the small lagenids. The first extinction pulse was synchronous at Liangfengya and Meishan, occurring at the top of the *C. yini* Zone. The second extinction pulse was possibly also synchronous, although this is less certain. Thus, conodont biozones from Liangfengya include *C. yini*, *C. meishanensis*, *H. preparvus*, and *H. parvus*. However, Yuan and Shen (2011) did not find conodonts from beds 21b to 22, and placed this interval in the *H. preparvus* Zone. However, in another section at Daijiagou ~50 km north of the Liangfengya section, *H. parvus* was found in the same interval (Yuan et al., 2015). So, the second extinction pulse at Liangfengya is within (or a little above) the *H. parvus* Zone. Besides, Peng and Tong (1999) claimed the claystone beds found at Liangfengya (bed 21b) and Meishan (bed 28) are contemporaneous, which further suggests that the second extinction of foraminifers in these two sections is synchronous.

### 6.3. A single, less devastating extinction pulse in basin settings

Data from basinal sections are insufficient for full evaluation of the precise levels of the extinction horizons. However, one main extinction pulse of lower magnitude (when compared to shallow settings, Fig. 13A) can be identified in the *C. yini* Zone. The main extinction pulse eliminated 63.0% of taxa (17/27, Fig. 5), which gradually disappear between the *C. yini* and *C. meishanensis* zones at Shangsi. This main extinction pulse corresponds to the extinction pulse in platform and the first pulse in slope settings. In addition, several species gradually disappeared in the PTB interval, but it is difficult to pinpoint the

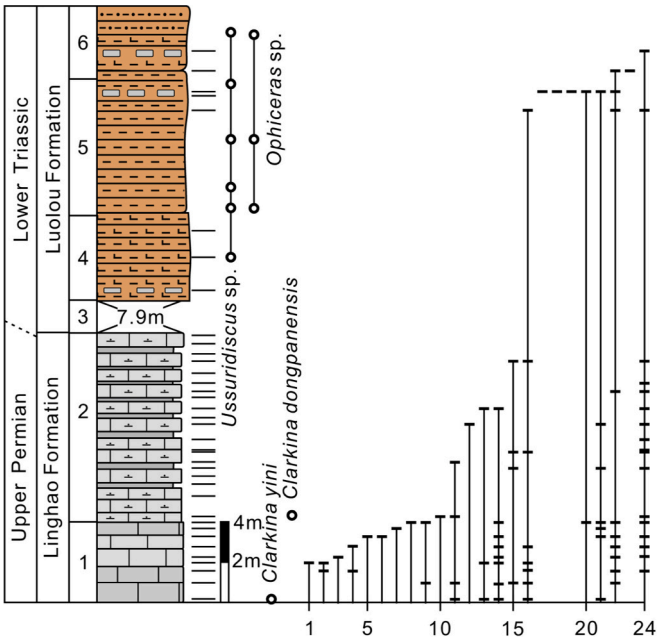


**Fig. 7.** Stratigraphic occurrences of foraminifers in the Sidahzai section. A list of foraminifers identified from Sidahzai is provided in a Supplementary Table.

second extinction pulse at Shangsi. Similarly, Gujiao and Sidazhai also record the main extinction in the *C. yini* Zone (the first occurrence of *C. yini* is below the main extinction interval) with 50% (9/18, Fig. 6) and 63.6% (14/22, Fig. 7) of taxa losses, respectively. In contrast to the platform area, 18 species are found in basinal strata from the PTB interval. The basinal fauna is dominated by small lagenids and a few Lazarus taxa. The basinal fauna did not suffer the second extinction pulse that occurred in slope settings. Additionally, diversity of the basinal fauna rebounded moderately in the late Griesbachian.

These three distinct extinction patterns suggest that the three palaeoenvironmental settings we have examined suffered different types and magnitudes of environmental fluctuations, and also different extinction and survival processes. Shallow platform dwellers were impacted by high temperatures. Basinal taxa suffered anoxia, whilst the mid water depths were influenced by both high temperatures and anoxia during the PTB interval (Song et al., 2014). The environments recorded by the Cili and Dajiang sections quickly became inhospitable. The deeper slope environments retained a habitable zone, and Liangfengya and Meishan shared similar foraminiferal assemblages and water depths during the PTB interval. Basinal environments were depauperate. As the temperature continued to rise (Fig. 14), the second extinction pulse occurred, forcing survivors to migrate into basinal settings where they were able to tolerate the poor oxygen levels while escaping from high temperatures (discussed below). Slope environments became uninhabitable for foraminifers by the late Griesbachian.

## 7. Selective extinction and survival

Selective extinction of marine invertebrates during the PTME has been proposed several times (Knoll et al., 1996; Clapham and Payne, 2011; Song et al., 2014) and was mostly a function of physiological selectivity. Taxa that lacked physiological buffering and non-motile taxa suffered markedly higher extinction rates (Knoll et al., 1996; Knoll et al., 2007). Similarly, taxa thought to be susceptible to anoxia and high temperatures also suffered higher extinction magnitudes. It follows that the survival or extinction of a taxon depends on how it was able to respond to these factors. The behaviours of foraminifera during the PTME exhibit high selectivity in both taxonomy and ecology, and they are, therefore, an informative group for evaluating different

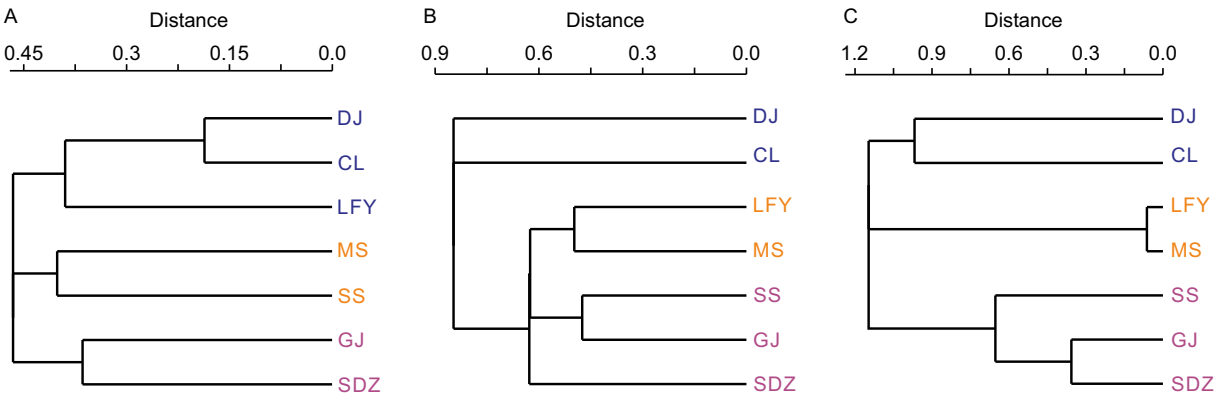


**Fig. 8.** Dendograms of Q-model cluster analyses of the seven sections, tested during the *C. yini* Zone (A), the PTB interval (B), and the late Griesbachian (C). Blue fonts represent platform foraminiferal assemblages. Orange-red fonts represent slope foraminiferal assemblages. Pink fonts represent basin foraminiferal assemblages. Abbreviations: DJ = Dajiang; CL = Cili; LFY = Liangfengya; MS = Meishan; SS = Shangsi; GJ = Gujiao; SDZ = Sidazhai. (For interpretation of the references to color in this figure legend, the reader is referred to the web version of this article.)

drivers of extinction.

### 7.1. Taxonomic selectivity

The Order Fusulinida experienced a severe extinction during the late Guadalupian (Capitanian, Middle Permian) mass extinction, and never re-established their Middle Permian levels of diversity (Stanley and Yang, 1994; Tong and Shi, 2000; Yang et al., 2004; Bond and Wignall, 2009). In the aftermath of that crisis, non-fusulinacean fusulinids rapidly came to dominate Lopingian assemblages in low palaeolatitudinal tropical shallow carbonate platform settings (Tong and Shi, 2000; Mohtat-Aghaï and Vachard, 2005; Kobayashi, 2006; Gaillot and Vachard, 2007). During the latest Permian extinction pulse, fusulinids suffered the greatest losses, and 92.3% of species became extinct (48/52, Fig. 13B). Those taxa with specialized ecological distribution, large tests, and complex morphology all vanished, including all fusulinacean fusulinids, all Palaeotextulariidae, and most Biseriamminidae (except *Globivalvulina bulloides*). In the PTB interval, the non-fusulinacean fusulinids comprise primitive forms such as *Diplosphaerina inaequalis* and *Earlandia* sp., and these are augmented by some moderately complex taxa such as *Globivalvulina bulloides* and *Neoendothyra* sp. During the second extinction pulse, most non-fusulinacean fusulinids (except the

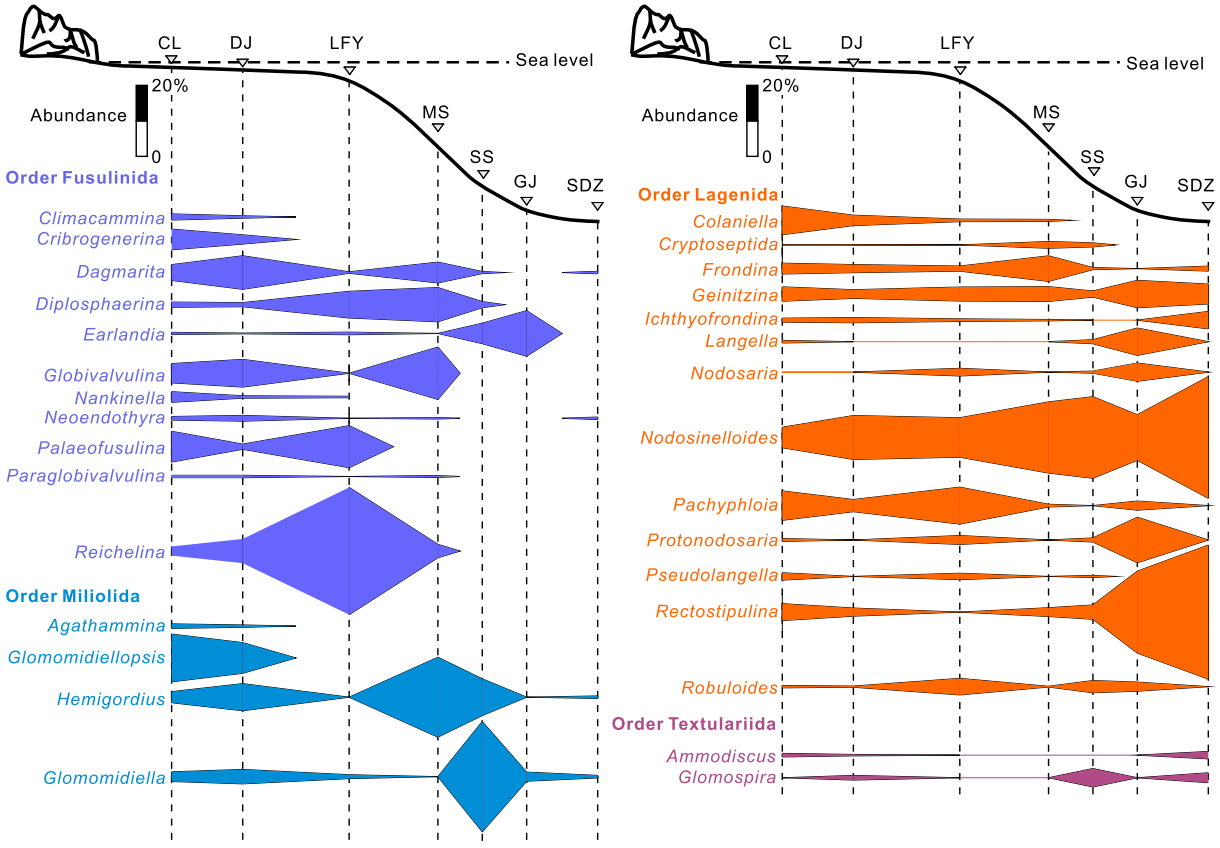


**Fig. 9.** A schematic diagram illustrating the percentage distribution of the dominant genera with depth in the late Changhsingian of South China. Abbreviations as in Fig. 8 caption. Indigo-blue boxes represent the Order Fusulinida. Orange boxes represent the Order Lagenida. Sky-blue boxes represent the Order Miliolida. Purple boxes represent the Order Textulariida. (For interpretation of the references to color in this figure legend, the reader is referred to the web version of this article.)

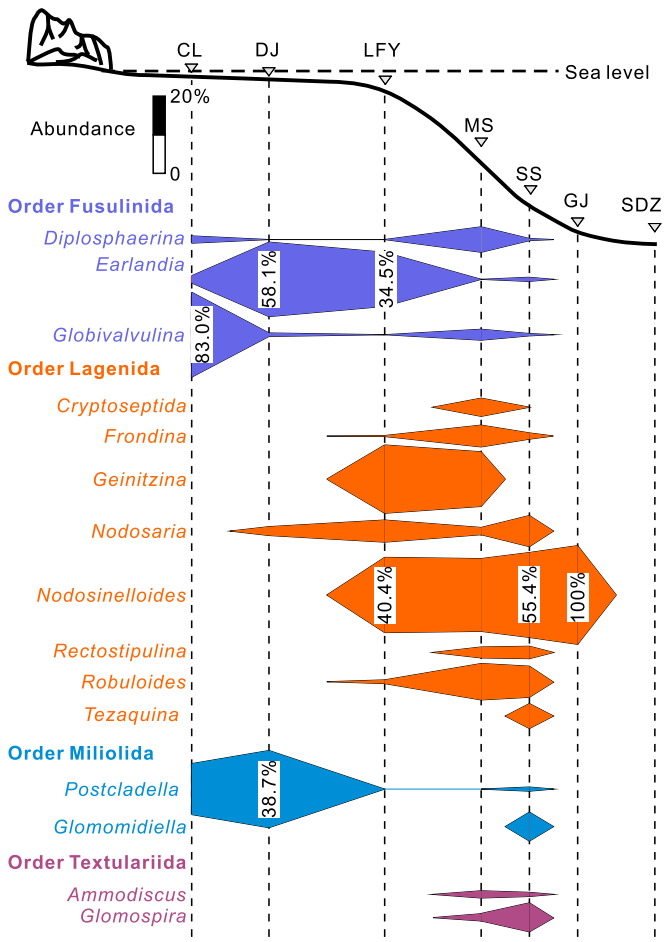


**Fig. 10.** The percentage distribution of dominant foraminifer genera with depth in the PTB interval in South China. Abbreviations as in Fig. 8 caption. Colours follow Fig. 9. (For interpretation of the references to color in this figure legend, the reader is referred to the web version of this article.)

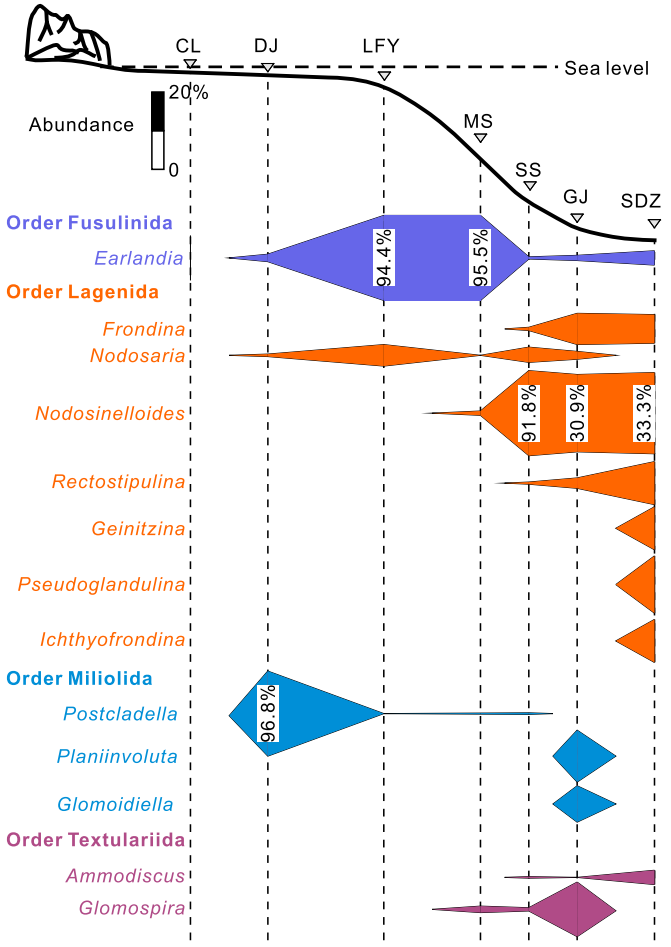


**Fig. 11.** The percentage distribution of dominant foraminifer genera with depth in the late Griesbachian of South China. Abbreviations as in Fig. 8 caption. Colours follow Fig. 9. (For interpretation of the references to color in this figure legend, the reader is referred to the web version of this article.)

disaster taxon *Earlandia* sp.) disappeared.

The Lagenida originated in the Late Carboniferous (Tappan and Loeblich, 1988; Groves et al., 2003) and underwent rapid expansion in inner to middle neritic environments throughout the Tethyan region and northern higher palaeolatitudes after the late Guadalupian mass extinction (Groves and Altiner, 2005). Most lagenids are generalists, which can tolerate and spread into various environments (Fig. 9). Among them, 63.3% (38/60, Fig. 13B) vanished during the first extinction pulse. The large lagenids (such as *Pachyphloia* and *Colaniella*) are characterized by thicker, stronger tests and these became extinct along with some other robust-walled taxa. The lagenids were moderately diverse in slope settings during the PTB interval, and these survivors are dominated by generalists with small flattened tests. The earliest Triassic extinction pulse accounted for 62.1% of the diversity loss (18/29). The second pulse chiefly affected palmate-shaped taxa such as *Geinitzina* and *Ichthyofrondina*, while the elongate and lanceolate tests such as *Nodosinelloides* and *Nodosaria* became more dominant in the late Griesbachian.

Miliolids first appeared at the beginning of the Pennsylvanian (Late Carboniferous) and proliferated rapidly in the Middle and Late Permian in Palaeotethys (Altiner et al., 2003; Jin and Yang, 2004). Miliolids are mostly members of the Superfamily Cornuspiroidea in the Late Permian, and they suffered 84.6% extinction (22/26) in the first extinction pulse. Miliolids include opportunists and some large, complex forms, such as *Glomomidiellopsis*, *Agathammina*, *Neodiscus*, *Multidiscus*, and *Neodiscopsis*, all prominent victims of the first pulse of extinction. Few miliolids survived into the PTB interval and these also suffered the second extinction pulse. In the late Griesbachian, miliolids comprised only four Lazarus taxa or opportunists (Kauffman and Harries, 1996). Textulariides are of low abundance and diversity in all our faunas and they were only slightly affected by the PTME, while three species emerged again in the late Griesbachian. The Involutinida includes one species, *Pseudovidalina* sp., which disappeared during the first extinction pulse.

### 7.2. Selective extinction of shallow-water dwellers

Here we divide foraminiferal species into two categories: shallow-water dwellers that are mainly seen on the platforms but occasionally also appear in the slope facies, and widespread types that are commonly seen in all three facies in the late Changhsingian. The shallow-water dwellers are mainly the fusulinids, large lagenids, and miliolids. Widespread types include the small lagenids and some generalists from other groups. There is a clear disparity in the extinction processes between these groups (Fig. 13C) because the shallow-water dwellers suffered one abrupt extinction in the first pulse and with 96.7% of losses (58/60 species). The single survivor, *Pseudolangella dorashamensis*, plus a new species, *Neoendothyra* sp., occur in slope settings during the PTB interval, but these eventually became extinct in the second extinction pulse. In contrast, the widespread elements lost 25% (4/16) and 33.3% (4/12) of diversity in the two extinction pulses, respectively. The first extinction pulse wiped out moderately complex and

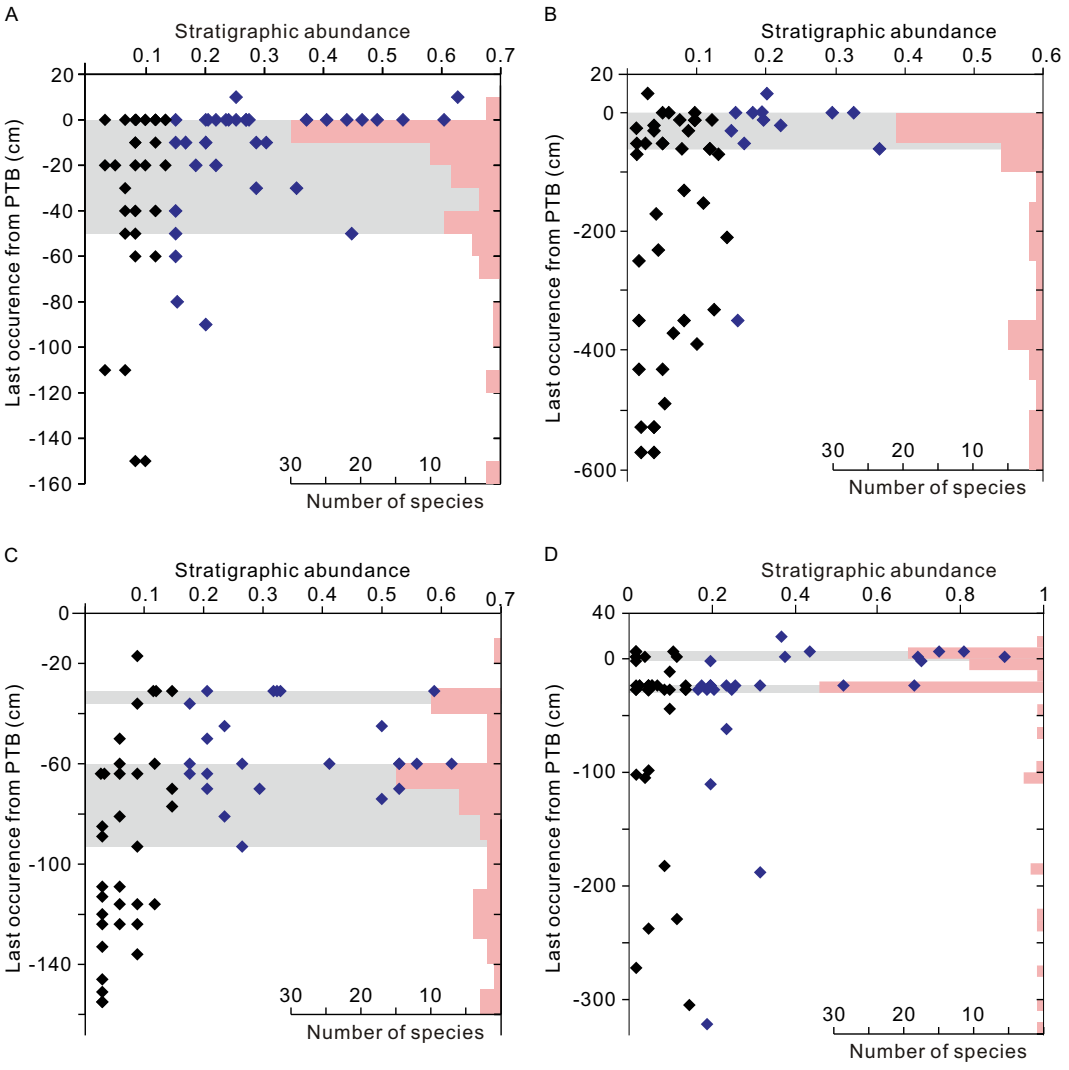


**Fig. 12.** Stratigraphic abundance versus last occurrence of the late Changhsingian foraminifer species from the Cili (A), Dajiang (B), Liangfengya (C), and Meishan (D) sections. Blue dots represent species with stratigraphic abundances > 15%. Pink boxes represent the number of species disappear or extinct within corresponding distance. Dajiang and Meishan are cited from Song et al. (2009b) and Song et al. (2009a), respectively. (For interpretation of the references to color in this figure legend, the reader is referred to the web version of this article.)

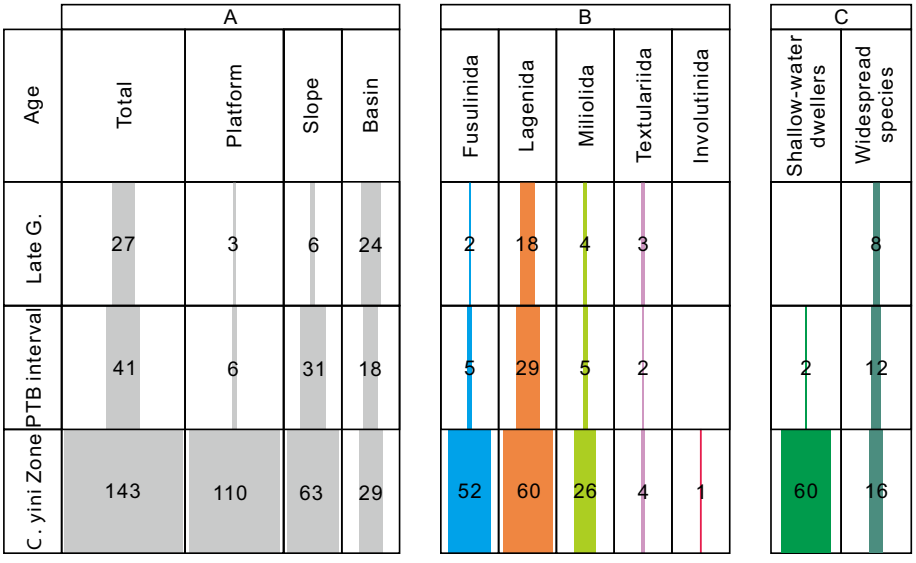


**Fig. 13.** Number of foraminifer species recorded from different (A) environments, (B) orders, and (C) types in South China from the late Changhsingian (*C. yini* Zone) to late Griesbachian. Shallow-water dwellers are mainly seen on the platforms but occasionally recognized in the slope facies. Widespread species are occurred in all three facies.

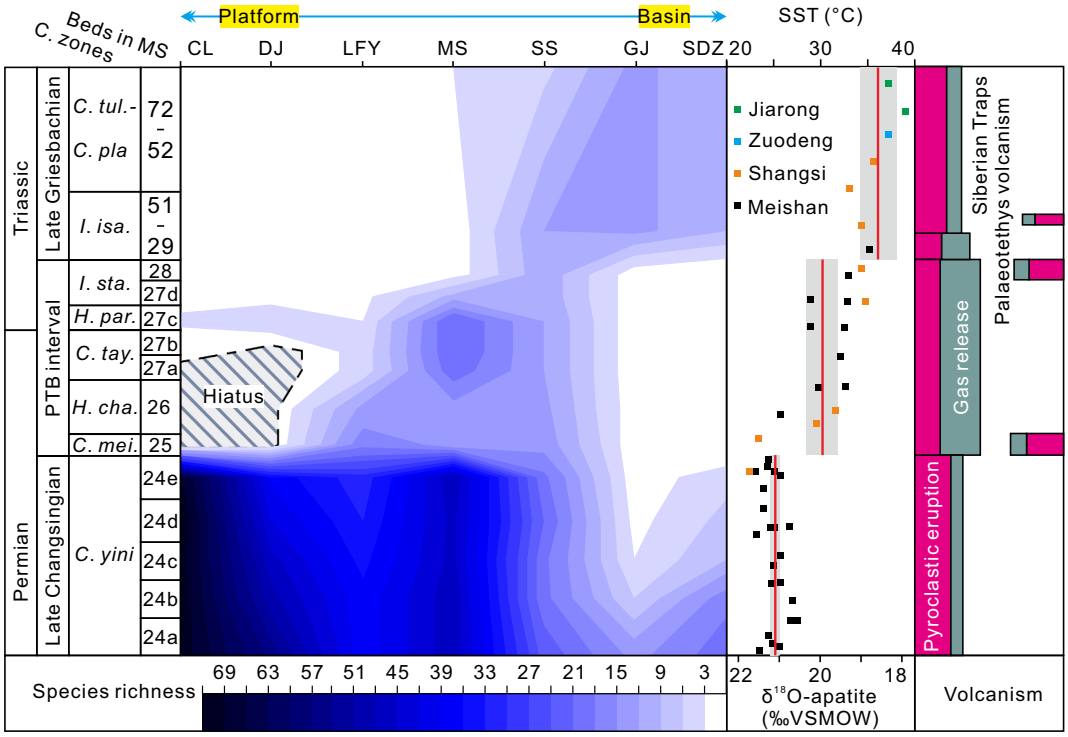


**Fig. 14.** The deep-ward migration of foraminifers during the PTME. Sea surface temperature data is from Joachimski et al. (2012) and Sun et al. (2012). Red lines and grey shadows represent the mean sea surface temperature and 95% confidence intervals in the three time bins. Volcanism events are from Burgess et al. (2017) and Yin and Song et al. (2013). Section abbreviations as in Fig. 8 caption; SST = sea surface temperature. (For interpretation of the references to color in this figure legend, the reader is referred to the web version of this article.)

robust taxa such as *Langella*, *Protonodosaria*, and *Hemigordius*, and resulted in the contraction of habitats into the slope area. Shortly after this, widespread types suffered the second extinction pulse, which saw the survivors remaining predominantly in deep basinal environments.

## 8. Deep-ward migration of foraminiferal diversity

### 8.1. Migration pattern

In the late Changhsingian, the hotspot of foraminiferal diversity was concentrated in shallow platform settings (Fig. 14) such as the Yangtze Platform and the Great Bank of Guizhou, where 110 species (76.4% of

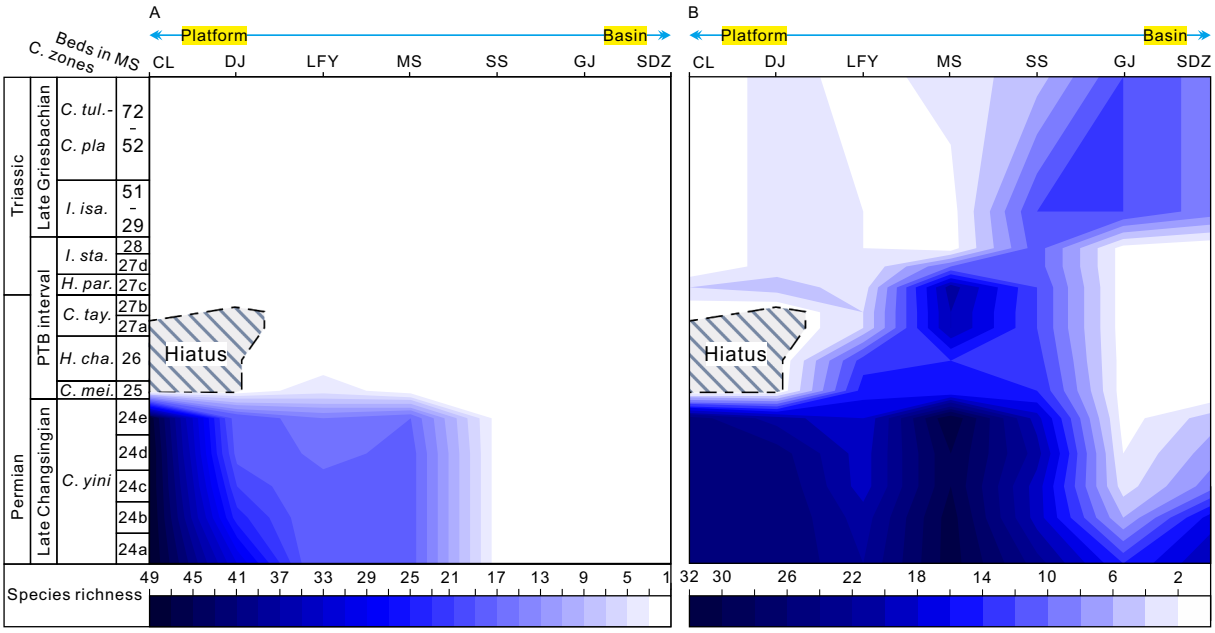


**Fig. 15.** The spatial and temporal distribution of (A) shallow-water and (B) other foraminiferal species during the Permian-Triassic transition. Abbreviations consistent with Fig. 14.

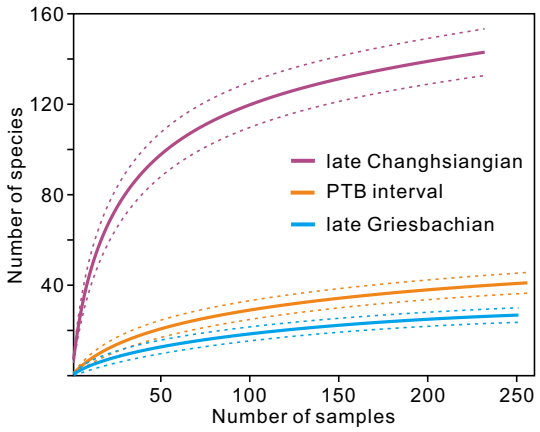


**Fig. 16.** Sample-based rarefaction curves for the late Changhsingian, the PTB interval, and the late Griesbachian intervals. The dashed lines represent 95% confidence intervals.

the then extant fauna), including all 19 fusulinacean species, are found. Deeper-water environments also had moderately diverse faunas in the late Changhsingian, with 63 (1 fusulinacean) and 29 (0 fusulinacean) species found in slope and basinal settings, accounting for 43.8% and 20.1% of the total fauna (note, some species exist in multiple settings). During the PTB interval, the diversity hotspot moved to the slopes, where 31 species (75.6% of the total fauna) were found. In contrast, platform (6 species) and basinal (18 species) settings yield only a few foraminifers in the PTB interval. The diversity hotspot continued its migration to deeper settings in the late Griesbachian, when basinal environments (24 species, 88.8% the total fauna) became much more diverse than on the slopes (6 species) and platforms (3 species, Fig. 13).

Our data reveal that the selective extinction of shallow-water taxa partly accounts for the initial migration of the diversity hotspot, as the disappearance of 58 shallow-water species caused a significant decline in biodiversity on the platforms (Fig. 15A). Although widespread types also suffered severe losses during the first pulse of extinction, over 30 species (including a few newcomers) are known from the PTB interval. In contrast to the pre-extinction interval, the survivors of the first extinction pulse preferred slope settings. By this time, shallow settings were occupied by a few disaster taxa, suggesting unfavourable conditions for most species. Similarly, the deep basinal environments were also depauperate in foraminifers. The transition of foraminiferal diversity hotspots from platform to slope settings may be explained in two ways. First, as discussed above, the selectivity of extinction may have played an important role; although shallow-water taxa apparently became "extinct" in those settings, some also lived in slope settings, where they survived. Second, the survivors in slope settings also included taxa known from both pre-extinction platform and basinal environments, suggesting that these taxa might have migrated to the slopes during extinction, such as *Pseudolangella dorashamensis* and *Neoendothyra* sp. During the second extinction pulse, the species (not recorded in basinal settings in the PTB interval) from the slope settings in the PTB interval disappeared (or become extinct) in the late Griesbachian, whilst the survivors from the PTB interval (such as *Frondina permica*, *Geinitzina spandeli*, *Nodosaria skyphica*, *Nodosinelloides sagitta*, and *Rectostipulina hexamerata*) and newcomers (such as *Nodosinelloides* sp. from Gujiao, *Frondina* sp. from Sidazhai) are only recorded in basinal settings in the late Griesbachian (Fig. 14). Ten species migrated from the slope settings into basinal environments in the late Griesbachian. The second transition of foraminiferal diversity hotspots was caused by the deep-ward migration of survivors of the second extinction pulse.

Subsample analysis shows that the decrease in biodiversity and the deep-ward migration of foraminifers between the Late Permian and Early Triassic is not the result of sampling bias. Sample-based rarefaction was performed on the late Changhsingian, PTB interval, and late Griesbachian data sets (Fig. 16). When the randomly subsampled number reaches 200, the diversity patterns in our three sample intervals are revealed to be complete. Sample-based rarefaction analysis was carried out for each facies within our three time bins (Fig. 17). When the random subsampled size reaches 50 samples, it turns out that some settings were insufficiently sampled, such as slope and basin settings in the late Changhsingian and the PTB interval. Nevertheless, the diversity hotspot retains its pattern in being located on the platforms in the late Changhsingian (100 species), on the slopes during the PTB interval (36 species), and in the basins during the late Griesbachian (18 species), We also performed individual-based rarefaction to test for sampling bias, the results of which further support our findings.

### 8.2. Triggers of deep-ward migration

Facies analysis suggests that sea-level change was not a key driver of the deep-ward migration of foraminifers during the PTB interval. The sections record a marine regression, and this affected the environment in the lower part of the PTB interval (equivalent to beds 25–27b at Meishan) in shallow settings, such as Dajiang and Cili, but the deeper-water sections were not influenced. Strata representing the upper part of the PTB interval (equivalent to beds 27c–28 at Meishan) are well documented in these sections, suggesting that sea level had risen by this time and re-established depositional environments similar to those of the Late Permian. Nevertheless, during the second pulse of extinction,

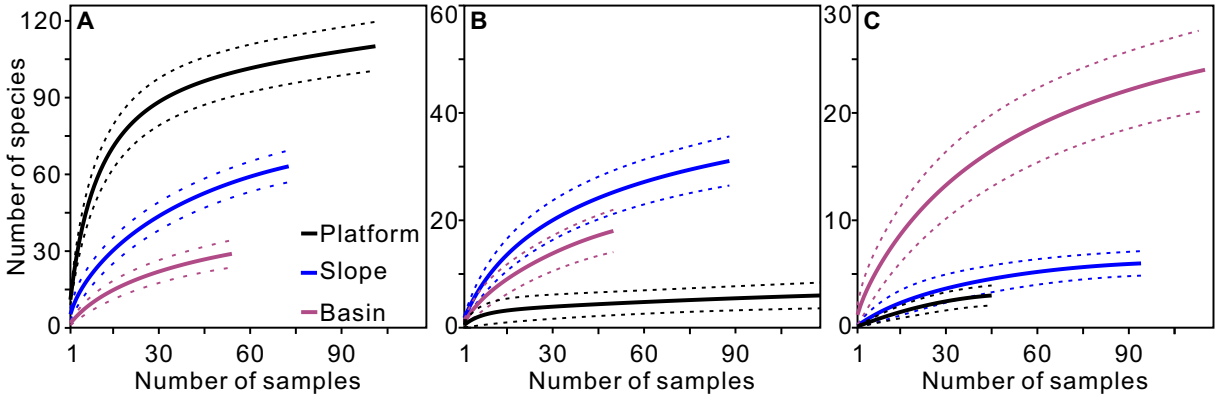


**Fig. 17.** Sample-based rarefaction curves for platform, slope, and basinal environments. (A) Rarefaction curves in the *C. yini* Zone. (B) Rarefaction curves in the PTB interval. (C) Rarefaction curves in the late Griesbachian. The black lines represent curves from the platform environment. The blue lines represent curves from slope environment. The blue-violet represent curves from the basin environment. The dashed lines represent 95% confidence intervals. (For interpretation of the references to color in this figure legend, the reader is referred to the web version of this article.)

the survivors migrated to basinal settings, which account for 88.8% of species.

The PTB mass extinction interval lasted ~30,000-60,000 years (Shen et al., 2018) and saw a ~10 °C rise in sea surface temperatures in equatorial regions (Sun et al., 2012). Such extreme warming represents a potentially potent driver of migration of foraminifers to deeper, cooler waters. Modern benthic foraminifers are considered eurythermal as they are found in oceans from the tropics to the polar regions. The upper thermal limit for most modern foraminifer species is usually < 35 °C (Nigam et al., 2008; Song et al., 2014), but experimental studies have demonstrated that the temperature range for reproduction is much narrower than that for individual growth and survival (Nigam et al., 2008; Saraswat et al., 2011). Thus, *Rosalina globularis* can survive temperatures from 20 °C to 35 °C, but reproduction only occurs at 25 °C (Saraswat et al., 2011). Overheating of surface waters during the PTB interval and late Griesbachian may have rendered them extremely unsuitable habitats for foraminifera. The survivors could have escaped the stress of high temperatures by migrating either horizontally (latitudinally) or vertically. For marine animals, vertical migration (if possible) is likely a more effective strategy than migration across the latitudes (Burrows et al., 2019). Climate modelling suggests that water temperatures at 200–400 m depth were 10–14 °C cooler than those in surface waters in equatorial regions during the PTB interval (Winguth et al., 2015). Deeper waters may also have been a refuge for other animals as well as foraminifers, such as conodonts, bivalves, and echinoids (Song et al., 2014; Godbold et al., 2017) during the crisis interval.

Toxic compounds released by the Siberian Traps large igneous province and minor volcanic activities around the Palaeotethys Ocean (Yin and Song, 2013; Burgess et al., 2017) (Fig. 14) are a further potential driver of foraminiferal migration. The Siberian Traps in particular released vast quantities of toxic compounds, including poisonous metals (Sanei et al., 2012), noxious gases (Keller and Kerr, 2014) and chars (Grasby et al., 2011), which might have transformed surface seawaters into a toxic soup in which foraminifers could barely survive. This would have been compounded by additional loading of potentially toxic products from massive soil erosion and/or biomass burning. In contrast, deeper waters were likely less affected by these products of volcanism. The harmful effects of these toxic compounds were probably "consumed" by those organisms that persisted in shallow waters (Grasby et al., 2017; Shen et al., 2019). A modern analogy for our scenario is Sorfjord in western Norway – one of the most metal-polluted fjords in the world – where benthic foraminifers have transferred their habitat to deeper waters just within their tolerance limits to escape toxicity in surface waters (Alve, 1991).

A great body of evidence supports the development of intense marine anoxia in both deep and shallow waters (within the photic zone) during the PTME interval (Wignall and Twitchett, 1996; Grice et al., 2005; Algeo et al., 2010). A major increase in the $\delta^{13}C$-depth gradient after the PTME suggests that deeper waters experienced more intense and prolonged oxygen restriction (Meyer et al., 2011). Observations on living foraminifers provide some clues about how they might have survived in low-oxygen conditions. Laboratory experiments show that the oxygen consumption rate increases significantly in foraminiferal specimens larger than 250 μm (Bradshaw, 1961), and we note that many of the surviving taxa were small (mostly < 200 μm). Furthermore, the elongate-tapered tests of survivors such as *Nodosinelloides*, *Nodosaria*, and *Geinitzina* possess higher surface area-to-volume ratios that likely improved mitochondrial oxygen uptake (Kaiho, 1994). It is also notable that many living foraminifers are capable of (even complete) denitrification (by using $NO_3^-$ for respiration rather than oxygen) enabling them to flourish in the oxygen minimum zone (Risgaard-Petersen et al., 2006). Culture experiments show that denitrification is an auxiliary metabolic mechanism for cell maintenance in many foraminiferal groups, including Lagenida, Miliolida, Textulariida, and Rotaliida (Piña-Ochoa et al., 2010). Further, denitrification has been shown to be a more efficient metabolism than aerobic respiration in some benthic foraminifers in the Peruvian oxygen minimum zone, and the ability of oxygen respiration still remains (Glock et al., 2019). Previous evidence indicates that intensive denitrification and/or anaerobic ammonium oxidation occurred during the PTME, and the foraminifera may play an important role in denitrification (Sun et al., 2019). It has been suggested that modern benthic foraminifera are responsible for up to 70 % of the total denitrification in several regions (Piña-Ochoa et al., 2010; Glock et al., 2013). Enhanced nitrogen fixation by cyanobacteria and other microbes has been suggested for the PTME (Luo et al., 2011), which may have continuously supplied nitrates to the anoxic water masses. Foraminifers living within the oxygen minimum zone, such as rotaliids, are able to store extremely high concentrations of nitrate seawater (several hundred times that of pore water) in large vacuoles for denitrification (Bernhard et al., 2012). Phylogenetic reconstruction of the enzymes' evolutionary history suggests an ancient acquisition of the foraminiferal denitrification pathway from prokaryote ancestors in the early Phanerozoic (Woehle et al., 2018). The evolution of hybrid respiration in foraminifera likely contributed to their ecological success in surviving during times of oxygen restriction and biotic crises such as the PTME.

Foraminifera have a higher tolerance of low oxygen levels than most other marine taxa (Song et al., 2014). Other hypoxia-tolerant groups include bivalves, gastropods, cephalopods, and corals, with bryozoans, echinoderms, ostracods, and non-ostracod crustaceans being much less tolerant. Predictions of survivorship, however, depend on complex interactions between oxygen level and temperature, with oxygen requirements of most animals increasing with temperature (Pörtner, 2010). However, the oxygen solubility of the seawater declined while temperatures rose during the PTME. Therefore, the oxygen requirement might be less in a cool water environment than a hot environment, and this might have been important for some taxa. Warming of the modern oceans and consequent loss of dissolved oxygen are reshaping the biogeography of some fishes and arthropods, forcing them to contract their ranges in the last few decades both vertically and poleward to occupy metabolically viable habitats (Deutsch et al., 2015). The vulnerability of marine organisms to hypoxia may cause them to migrate or even become extinct before reaching the temperature threshold (Pörtner and Knust, 2007). Physiological and ecological simulations of the PTME show that organisms with higher temperature sensitivity (some taxa among arthropods and chordates) may have vacated habitats in shallow areas at low latitudes (Penn et al., 2018). Physiological evidence suggests that some invertebrates, such as sipunculids, annelids or bivalves, possess an alternative mitochondrial oxidase in aerobic respiration (Buchner et al., 2001). The alternative oxidase may represent an ancient mechanism to tolerate oxygen-poor environments, and this is still prevalent in some invertebrates in hypoxic environments (Pörtner, 2010). Notably, taxa with high temperature tolerances, such as ostracods and gastropods, were able to survive in the shallow waters in the earliest Triassic, and these are major components of the microbialite.

## 9. Conclusion

A total of 13,422 individual foraminiferal specimens belonging to 173 species in 62 genera have been analyzed from seven different paleoenvironmental settings across the Permian-Triassic boundary in South China. Three foraminiferal faunas, from the late Changhsingian, the Permian-Triassic boundary interval, and the late Griesbachian, were identified, and these are separated by two pulses of the PTME. These three faunas reveal that the foraminiferal diversity hotspot moved from shallow platforms to deeper slopes and finally into basinal settings during the PTME within ~30,000-60,000 years. Quantitative analysis presents three extinction patterns: 1) shallow sections exhibit one abrupt extinction pulse with 97.3% of species lost; 2) slope settings experienced two stepwise extinction pulses, in which 63.5% and 90.5%

of total taxa became extinct; 3) basin dwellers suffered one main extinction pulse in which > 50% of species were lost. The selective extinction of foraminifers reveals that both large and complex-morphology taxa (such as fusulinids) and shallow water dwellers were prominent victims of the first extinction pulse. We suggest that the deep-ward shift in diversity was a strategy to avoid overheated and toxic shallow waters that resulted from intense volcanic activity in the Siberian Traps and coeval volcanism around the Palaeotethys Ocean. This ecological strategy for escaping the deadly drivers of extinction may provide a key to understanding how some marine species survived this catastrophic crisis and how modern ocean dwellers might escape warming oceans in the coming decades.

## Declaration of competing interest

The authors declare that they have no known competing financial interests or personal relationships that could have appeared to influence the work reported in this paper.

## Acknowledgements

We thank Xu Dai and Enhao Jia for their help in the field, Ruoyu Bai for conodont biostratigraphy, and Lirong Yang for identification of foraminifera. This study is supported by the National Natural Science Foundation of China (41821001, 41622207, 41530104, and 41661134047), the State Key R&D Project of China (2016YFA0601100), the Strategic Priority Research Program of Chinese Academy of Sciences (No. XDB26000000), and the UK Natural Environment Research Council's Eco-PT project (NE/P01377224/1) and Advanced Research Fellowship (NE/J01799X/1). This study is a contribution to the IGCP 630 project.

## Appendix A. Supplementary data

Supplementary data to this article can be found online at https://doi.org/10.1016/j.earscirev.2020.103329.

## References

Aghai, P.M., Vachard, D., Krainer, K., 2009. Transported foraminifera in Palaeozoic deep red nodular limestones exemplified by latest Permian Neoendothyra in the Zal section (Julfa area, NW Iran). Rev. Esp. Micropaleontol. 41 (1–2), 197–213.
Algeo, T.J., Hinnov, L., Moser, J., Maynard, J.B., Elswick, E., Kuwahara, K., Sano, H., 2010. Changes in productivity and redox conditions in the Panthalassic Ocean during the latest Permian. Geology 38 (2), 187–190.
Alroy, J., Aberhan, M., Bottjer, D.J., Foote, M., Fürsich, F.T., Harries, P.J., Hendy, A.J., Holland, S.M., Ivany, L.C., Kiessling, W., 2008. Phanerozoic trends in the global diversity of marine invertebrates. Science 321 (5885), 97–100.
Altiner, D., 1981. Le Trias dans la region de Pinarbasi, Taurus oriental, Turqui: unites lithologiques, micropaleontologie, milieux de depot. Riv. Ital. Paleontol. Stratigr. 86 (4), 705–738.
Altiner, D., 2013. Evolutionary changes in Changsingian foraminifera: extinction and post-extinction recovery. Acta Geol. Sin. 87 (supp), 897–899.
Altiner, D., Altiner, S.Ö., 2010. *Danielita gailloti* n. gen., n. sp., within the evolutionary framework of Middle-Late *Permian dagmaritins*. Turk. J. Earth Sci. 19 (4), 497–512.
Altiner, D., Baud, A., Guex, J., Stampfli, G., 1980. La limite Permien-Trias dans quelques localités do Moyen-Orient: recherches stratigraphiques et micropaléontologique. Riv. Ital. Paleontol. 85, 683–714.
Altiner, D., Özkan-Altiner, S., Koçyiğit, A., 2000. Late Permian foraminiferal biofacies belts in Turkey: palaeogeographic and tectonic implications. Geol. Soc. Lond., Spec. Publ. 173 (1), 83–96.
Altiner, D., Savini, R., Özkan-Altiner, S., 2003. Morphological variation in *Hemigordius harltoni* Cushman & Waters, 1928: remarks on the taxonomy of Carboniferousand Permian hemigordiopsids. Riv. Ital. Paleontol. Stratigr. 109 (2), 195–211.
Alve, E., 1991. Benthic foraminifera in sediment cores reflecting heavy metal pollution in Sorfjord, western Norway. J. Foraminifer. Res. 21 (1), 1–19.
Angiolini, L., Checconi, A., Gaetani, M., Rettori, R., 2010. The latest Permian mass extinction in the Alborz Mountains (north Iran). Geol. J. 45 (2–3), 216–229.
Armstrong, H.A., Brasier, M.D., Armstrong, H.A., Brasier, M.D., 2004. Foraminifera, Microfossils. Blackwell Publishing, pp. 142–187.
Beavington-Penney, S.J., Racey, A., 2004. Ecology of extant nummulitids and other larger benthic foraminifera: applications in palaeoenvironmental analysis. Earth-Sci. Rev. 67 (3), 219–265.
Benton, M.J., 2018. Hyperthermal-driven mass extinctions: killing models during the Permian–Triassic mass extinction. Philos. Trans. R. Soc. A Math. Phys. Eng. Sci. 376 (2130) 20170076.
Bernhard, J.M., Edgcomb, V.P., Casciotti, K.L., McIlvin, M.R., Beaudoin, D.J., 2012. Denitrification likely catalyzed by endobionts in an allogromiid foraminifer. ISME J. 6 (5), 951–960.
Bond, D.P.G., Wignall, P.B., 2009. Latitudinal selectivity of foraminifer extinctions during the late Guadalupian crisis. Paleobiology 35 (4), 465–483.
Bond, D.P.G., Wignall, P.B., 2010. Pyrite framboid study of marine Permian-Triassic boundary sections: a complex anoxic event and its relationship to contemporaneous mass extinction. Geol. Soc. Am. Bull. 122 (7–8), 1265–1279.
Bradshaw, J.S., 1961. Laboratory experiments on the ecology of foraminifera. Cushman Found. Foram. Res. Contr. 17, 87–106.
Brasier, M.D., 1995. Fossil indicators of nutrient levels. 2: evolution and extinction in relation to oligotrophy. Geol. Soc. Lond. Spec. Publ. 83 (1), 133–150.
Buchner, T., Abele, D., Pörtner, H.-O., 2001. Oxyconformity in the intertidal worm Sipunculus nudus: the mitochondrial background and energetic consequences. Comp. Biochem. Physiol. B: Biochem. Mol. Biol. 129 (1), 109–120.
Burgess, S.D., Muirhead, J.D., Bowring, S.A., 2017. Initial pulse of Siberian Traps sills as the trigger of the end-Permian mass extinction. Nat. Commun. 8 (1), 164.
Burrows, M.T., Bates, A.E., Costello, M.J., Edwards, M., Edgar, G.J., Fox, C.J., Halpern, B.S., Hiddink, J.G., Pinsky, M.L., Batt, R.D., García Molinos, J., Payne, B.L., Schoeman, D.S., Stuart-Smith, R.D., Poloczanska, E.S., 2019. Ocean community warming responses explained by thermal affinities and temperature gradients. Nat. Clim. Chang. 9 (12), 959–963.
Cao, C., Zheng, Q., 2007. High-resolution lithostratigraphy of the Changhsingian stage in Meishan section D, Zhejiang. J. Stratigr. 31, 14–22.
Cao, C., Zheng, Q., 2009. Geological event sequences of the Permian-Triassic transition recorded in the microfacies in Meishan section. Sci. China Ser. D Earth Sci. 52 (10), 1529–1536.
Chan, S.A., Kaminski, M.A., Al-Ramadan, K., Babalola, L.O., 2017. Foraminiferal biofacies and depositional environments of the Burdigalian mixed carbonate and siliciclastic Dam Formation, Al-Lidam area, Eastern Province of Saudi Arabia. Palaeogeogr. Palaeoclimatol. Palaeoecol. 469, 122–137.
Chen, Z.Q., Kaiho, K., George, A.D., 2005. Survival strategies of brachiopod faunas from the end-Permian mass extinction. Palaeogeogr. Palaeoclimatol. Palaeoecol. 224 (1–3), 232–269.
Chen, Z., Tong, J., Kaiho, K., Kawahata, H., 2007. Onset of biotic and environmental recovery from the end-Permian mass extinction within 1–2 million years: a case study of the Lower Triassic of the Meishan section, South China. Palaeogeogr. Palaeoclimatol. Palaeoecol. 252 (1–2), 176–187.
Chen, Z.Q., Yang, H., Luo, M., Benton, M.J., Kaiho, K., Zhao, L., Huang, Y., Zhang, K., Fang, Y., Jiang, H., 2015. Complete biotic and sedimentary records of the Permian–Triassic transition from Meishan section, South China: ecologically assessing mass extinction and its aftermath. Earth Sci. Rev. 149, 67–107.
Chu, D., Grasby, S.E., Song, H., Dal Corso, J., Wang, Y., Mather, T.A., Wu, Y., Song, H., Shu, W., Tong, J., 2020. Ecological disturbance in tropical peatlands prior to marine Permian-Triassic mass extinction. Geology 48 (3), 288–292.
Clapham, M.E., Payne, J.L., 2011. Acidification, anoxia, and extinction: a multiple logistic regression analysis of extinction selectivity during the Middle and Late Permian. Geology 39 (11), 1059–1062.
Clarkson, M., Kasemann, S., Wood, R., Lenton, T., Daines, S., Richoz, S., Ohnemueller, F., Meixner, A., Poulton, S., Tipper, E., 2015. Ocean acidification and the Permo-Triassic mass extinction. Science 348 (6231), 229–232.
Collin, P.Y., Kershaw, S., Crasquin-Soleau, S., Feng, Q., 2009. Facies changes and diagenetic processes across the Permian–Triassic boundary event horizon, Great Bank of Guizhou, South China: a controversy of erosion and dissolution. Sedimentology 56 (3), 677–693.
Colwell, R.K., Mao, C.X., Chang, J., 2004. Interpolating, extrapolating, and comparing incidence-based species accumulation curves. Ecology 85 (10), 2717–2727.
Colwell, R.K., Chao, A., Gotelli, N.J., Lin, S.-Y., Mao, C.X., Chazdon, R.L., Longino, J.T., 2012. Models and estimators linking individual-based and sample-based rarefaction, extrapolation and comparison of assemblages. J. Plant Ecol. 5 (1), 3–21.
Cowen, R., 1983. Algal symbiosis and its recognition in the fossil record. In: Tevesz, M.J.S., McCall, P.L. (Eds.), Biotic Interactions in Recent and Fossil Benthic Communities. Springer US, Boston, MA, pp. 431–478.
Crasquin, S., Forel, M.-B., Qinglai, F., Aihua, Y., Baudin, F., Collin, P.-Y., 2010. Ostracods (Crustacea) through the Permian-Triassic boundary in South China: the Meishan stratotype (Zhejiang Province). J. Syst. Palaeontol. 8 (3), 331–370.
Dai, X., Song, H., Brayard, A., Ware, D., 2018a. A new Griesbachian–Dienerian (Induan, Early Triassic) ammonoid fauna from Gujiao, South China. J. Paleontol. 93 (1), 48–71.
Dai, X., Song, H., Wignall, P.B., Jia, E., Bai, R., Wang, F., Chen, J., Tian, L., 2018b. Rapid biotic rebound during the late Griesbachian indicates heterogeneous recovery patterns after the Permian-Triassic mass extinction. GSA Bull. 130 (11–12), 2015–2030.
Deutsch, C., Ferrel, A., Seibel, B., Pörtner, H.-O., Huey, R.B., 2015. Climate change tightens a metabolic constraint on marine habitats. Science 348 (6239), 1132–1135.
Erwin, D.H., 1994. The Permo–Triassic extinction. Nature 367 (6460), 231–236.
Feng, Z., 1997. Lithofacies palaeogeography of the Early and Middle Triassic of south China. Chin. J. Geol. 32 (2), 212–220.
Feng, Q., Gu, S., 2002. Uppermost Changxingian (Permian) Radiolarian fauna from Southern Guizhou, Southwestern China. J. Paleontol. 76 (5), 797–809.
Feng, Z., He, Y., Wu, S., 1993. Lithofacies paleogeography of Permian of Middle and Lower Yangtze region. Acta Sedimentol. Sin. 11 (3), 13–24.
Feng, Q., Yang, F., Zhang, Z., Zhang, N., Gao, Y., Wang, Z., 2000. Radiolarian evolution during the Permian and Triassic transition in South and Southwest China. Dev.

Palaeontol. Stratigr. 18, 309–326.
Forel, M.-B., 2012. Ostracods (Crustacea) associated with microbialites across the Permian-Triassic boundary in Dajiang (Guizhou Province, south China). Eur. J. Taxon. 19, 1–34.
Forel, M.-B., 2013. The Permian–Triassic mass extinction: ostracods (Crustacea) and microbialites. Compt. Rendus Geosci. 345 (4), 203–211.
Forsey, G.F., 2013. Fossil evidence for the escalation and origin of marine mutualisms. J. Nat. Hist. 47 (25-28), 1833–1864.
Foster, W., Lehrmann, D., Yu, M., Ji, L., Martindale, R., 2018. Persistent environmental stress delayed the recovery of marine communities in the aftermath of the latest Permian mass extinction. Paleoceanogr. Paleoclimatol. 33 (4), 338–353.
Foster, W.J., Lehrmann, D.J., Yu, M., Martindale, R.C., 2019. Facies selectivity of benthic invertebrates in a Permian/Triassic boundary microbialite succession: implications for the “microbialite refuge” hypothesis. Geobiology 17 (5), 523–535.
Gaillot, J., Vachard, D., 2007. The Khuff Formation (Middle East) and time-equivalents in Turkey and South China: biostratigraphy from Capitanian to Changhsingian times (Permian), new foraminiferal taxa, and palaeogeographical implications. Coloquios Paleontol. 57 (57), 37–223.
Gaillot, J., Vachard, D., Galfetti, T., Martini, R., 2009. New latest Permian foraminifers from Laren (Guangxi Province, South China): palaeobiogeographic implications. Geobios 42 (2), 141–168.
Gallagher, S.J., 1998. Controls on the distribution of calcareous Foraminifera in the Lower Carboniferous of Ireland. Mar. Micropaleontol. 34 (3–4), 187–211.
Gao, Y.Q., Yang, F.Q., Peng, Y.Q., 2001. Late Permian deep water stratigraphy in Shaiwa of Ziyun, Guizhou. J. Stratigr. 25 (2), 116–124.
Glock, N., Schönfeld, J., Eisenhauer, A., Hensen, C., Mallon, J., Sommer, S., 2013. The role of benthic foraminifera in the benthic nitrogen cycle of the Peruvian oxygen minimum zone. Biogeosciences 10 (7), 4767–4783.
Glock, N., Roy, A.-S., Romero, D., Wein, T., Weissenbach, J., Revsbech, N.P., Høgslund, S., Clemens, D., Sommer, S., Dagan, T., 2019. Metabolic preference of nitrate over oxygen as an electron acceptor in foraminifera from the Peruvian oxygen minimum zone. Proc. Natl. Acad. Sci. U. S. A. 116 (8), 2860–2865.
Godbold, A., Schoepfer, S., Shen, S., Henderson, C.M., 2017. Precarious ephemeral refugia during the earliest Triassic. Geology 45 (7), 607–610.
Grasby, S.E., Sanei, H., Beauchamp, B., 2011. Catastrophic dispersion of coal fly ash into oceans during the latest Permian extinction. Nat. Geosci. 4 (2), 104–107.
Grasby, S.E., Shen, W., Yin, R., Gleason, J.D., Blum, J.D., Lepak, R.F., Hurley, J.P., Beauchamp, B., 2017. Isotopic signatures of mercury contamination in latest Permian oceans. Geology 45 (1), 55–58.
Grice, K., Cao, C., Love, G.D., Böttcher, M.E., Twitchett, R.J., Grosjean, E., Summons, R.E., Turgeon, S.C., Dunning, W., Jin, Y., 2005. Photic zone euxinia during the Permian-Triassic superanoxic event. Science 307 (5710), 706–709.
Groves, J.R., Altiner, D., 2005. Survival and recovery of calcareous foraminifera pursuant to the end-Permian mass extinction. C. R. Palevol 4 (6), 487–500.
Groves, J.R., Yue, W., 2009. Foraminiferal diversification during the late Paleozoic ice age. Paleobiology 35 (3), 367–392.
Groves, J.R., Altiner, D., Rettori, R., 2003. Origin and early evolutionary radiation of the Order Lagenida (Foraminifera). J. Paleontol. 77 (5), 831–843.
Groves, J.R., Altiner, D., Rettori, R., 2005. Extinction, survival, and recovery of lagenide foraminifers in the Permian–Triassic boundary interval, Central Taurides, Turkey. J. Paleontol. 79 (Jul 2005), 1–38.
Groves, J.R., Payne, J.L., Altiner, D., 2007. End-Permian mass extinction of lagenide foraminifers in the Southern Alps (Northern Italy). J. Paleontol. 81 (3), 415–434.
Gu, S., Feng, Q.L., He, W., 2007. The last permian deep-water fauna: latest Changhsingian small foraminifers from Southwestern Guangxi, South China. Micropaleontology 53 (4), 311–330.
Hammer, Ø., Harper, D.A.T., 2006. Paleontological Data Analysis. Blackwell Publishing, Oxford.
Hammer, Ø., Harper, D., Ryan, P., 2017. PAST: Paleontological Statistics. Version 3.16. National History Museum, University of Oslo, Oslo 256 pp.
He, W., Feng, Q., Gu, S., JIn, Y., 2005. Changxingian (Upper Permian) Radiolarian Fauna from Meishan D Section, Changxing, Zhejiang, China, and its possible paleoecological significance. J. Paleontol. 79 (2), 209–218.
He, Y., Luo, J., Wen, Z., Liu, M., Wang, Y., 2013. Lithofacies Palaeogeography of the Upper Permian Changxing Stage in the Middle and Upper Yangtze Region. Elsevier, China.
Hemleben, C., Kaminski, M.A., Kuhnt, W., Scott, D.B., 1990. Paleoecology, Biostratigraphy, Paleoceanography and Taxonomy of Agglutinated Foraminifera, 327. Kluwer Academic Publishers 1017 pp.
Hinojosa, J.L., Brown, S.T., Chen, J., Depaolo, D.J., Paytan, A., Shen, S., Payne, J.L., 2012. Evidence for end-Permian ocean acidification from calcium isotopes in biogenic apatite. Geology 40 (8), 743–746.
Hips, K., Pelikán, P., 2002. Lower Triassic shallow marine succession in the Bükk Mountains, NE Hungary. Geol. Carpath. 53 (6), 351–367.
Huang, Y., 2014. Extinction and Recovery of Bivalves During the Permian-Triassic Transition. Ph.D. Thesis. China University of Geosciences, Wuhan 136 pp.
Huang, Y., Tong, J., Fraiser, M.L., 2018. A Griesbachian (Early Triassic) mollusc fauna from the Sidazhai section, Southwest China, with paleoecological insights on the proliferation of genus Claraia (Bivalvia). J. Earth Sci. 29 (4), 794–805.
Insalaco, E., Virgone, A., Courme, B., Gaillot, J., Kamali, M.R., Moallemi, A., Lotfpour, M., Monibi, S., 2006. Upper Dalan Member and Kangan Formation between the Zagros Mountains and offshore Fars, Iran: depositional system, biostratigraphy and stratigraphic architecture. GeoArabia 11 (2), 75–176.
Isozaki, Y., 1997. Permo-Triassic boundary superanoxia and stratified superocean: records from lost deep sea. Science 276 (5310), 235–238.
Ji, W., 2012. Lower-Middle Triassic Conodont Biostratigraphy in Slope-Basin Facies, South Guizhou. Thesis. China University of Geosciences, Wuhan 48 pp.
Jia, E., Song, H., 2018. End-Permian mass extinction of calcareous algae and microproblematica from Liangfengya, South China. Geobios 51 (5), 401–418.
Jiang, H., Lai, X., Luo, G., Aldridge, R., Zhang, K., Wignall, P., 2007. Restudy of conodont zonation and evolution across the P/T boundary at Meishan section, Changxing, Zhejiang, China. Glob. Planet. Chang. 55 (1), 39–55.
Jiang, H., Lai, X., Yan, C., Aldridge, R.J., Wignall, P., Sun, Y., 2011. Revised conodont zonation and conodont evolution across the Permian–Triassic boundary at the Shangsi section, Guangyuan, Sichuan, South China. Glob. Planet. Chang. 77 (3–4), 103–115.
Jiang, H., Lai, X., Sun, Y., Wignall, P.B., Liu, J., Yan, C., 2014. Permian-Triassic conodonts from Dajiang (Guizhou, South China) and their implication for the age of microbialite deposition in the aftermath of the End-Permian mass extinction. J. Earth Sci. 25 (3), 413–430.
Jin, R., 1987. Radiolarites and sedimentary environments of the Late Permian Dalong Formation in the Northern sector of The Longmen Mountains, Sichuan Province. Geol. Rev. 33 (3), 238–246.
Jin, X., Yang, X., 2004. Paleogeographic implications of the Shanita-Hemigordius fauna (Permian foraminifer) in the reconstruction of Permian Tethys. Episodes 27 (4), 273–278.
Jin, Y., Wang, Y., Wang, W., Shang, Q., Cao, C., Erwin, D., 2000. Pattern of marine mass extinction near the Permian-Triassic boundary in South China. Science 289 (5478), 432–436.
Joachimski, M.M., Lai, X., Shen, S., Jiang, H., Luo, G., Chen, B., Chen, J., Sun, Y., 2012. Climate warming in the latest Permian and the Permian-Triassic mass extinction. Geology 40 (3), 195–198.
Kaiho, K., 1994. Benthic foraminiferal dissolved-oxygen index and dissolved-oxygen levels in the modern ocean. Geology 22 (8), 719–722.
Kauffman, E.G., Harries, P.J., 1996. The importance of crisis progenitors in recovery from mass extinction. Geol. Soc. Lond., Spec. Publ. 102 (1), 15–39.
Keller, G., Kerr, A.C., 2014. Volcanism, Impacts, and Mass Extinctions: Causes and Effects. Vol. 505 Geological Society of America 491 pp.
Knoll, A.H., Bambach, R.K., Canfield, D.E., Grotzinger, J.P., 1996. Comparative earth history and Late Permian mass extinction. Science 273 (5274), 452.
Knoll, A.H., Bambach, R.K., Payne, J.L., Pruss, S., Fischer, W.W., 2007. Paleophysiology and end-Permian mass extinction. Earth Planet. Sci. Lett. 256 (3–4), 295–313.
Kobayashi, F., 1997. Upper Permian foraminifers from the Iwai-Kanyo area, West Tokyo, Japan. J. Foram. Res. 27 (3), 186–195.
Kobayashi, F., 2006. Latest Permian (Changhsingian) foraminifers in the Mikata area, Hyogo—Late Paleozoic and Early Mesozoic foraminifers of Hyogo, Japan, Part 3. Nat. Hum. Act. 10, 15–24.
Kobayashi, F., 2012. Middle and Late Permian Foraminifers from the Chichibu Belt, Takachiho Area, Kyushu, Japan: implications For Faunal Events PERMIAN FORAMINIFERS OF TAKACHIHO. J. Paleontol. 86 (4), 669–687.
Kobayashi, F., 2013. Late Permian (Lopingian) foraminifers from the Tsukumi Limestone, southern Chichibu Terrane of eastern Kyushu, Japan. J. Foraminifer. Res. 43 (2), 154–169.
Kobayashi, F., Ishii, K.-I., 2003. Paleobiogeographic analysis of Yahtashian to Midian fusulinacean faunas of the Surmaq Formation in the Abadeh region, central Iran. J. Foraminifer. Res. 33 (2), 155–165.
Kolar-Jurkovšek, T., Vuks, V.J., Aljinović, D., Hautmann, M., Kaim, A., Jurkovšek, B., 2013. Olenekian (Early Triassic) fossil assemblage from eastern Julian Alps (Slovenia). Ann. Soc. Geol. Pol. 213–227.
Kolodka, C., Vennin, E., Vachard, D., Trocme, V., Goodarzi, M.H., 2012. Timing and progression of the end-Guadalupian crisis in the Fars province (Dalan Formation, Kuh-e Gakhum, Iran) constrained by foraminifers and other carbonate microfossils. Facies 58 (1), 131–153.
Lai, X., Yang, F.Q., Hallam, A., Wignall, P.B., 1996. The Shangsi section, candidate of the global stratotype section and point of the Permian–Triassic boundary. In: Yin, H. (Ed.), The Palaeozoic–Mesozoic Boundary, Candidates of the Global Stratotype Section and Point of the Permian–Triassic Boundary. China University of Geosciences Press, Wuhan, pp. 113–124.
Lee, J., Hallock, P., 1987. Algal Symbiosis as the Driving Force in the Evolution of Larger Foraminifera a. Ann. N. Y. Acad. Sci. 503, 330–347 Endocytobiology.
Lee, J., McEnery, M., Kahn, E., Schuster, F., 1979. Symbiosis and the evolution of larger foraminifera. Micropaleontology 25 (2), 118–140.
Lee, J.J., Cervasco, M.H., Morales, J., Billik, M., Fine, M., Levy, O., 2010. Symbiosis drove cellular evolution. Symbiosis 51 (1), 13–25.
Lehrmann, D.J., 1999. Early Triassic calcimicrobial mounds and biostromes of the Nanpanjiang basin, south China. Geology 27 (4), 359–362.
Lehrmann, D.J., Wei, J., Enos, P., 1998. Controls on facies architecture of a large Triassic carbonate platform; the Great Bank of Guizhou, Nanpanjiang Basin, South China. J. Sediment. Res. 68 (2), 311–326.
Lehrmann, D.J., Payne, J.L., Felix, S.V., Dillett, P.M., Wang, H., Yu, Y., Wei, J., 2003. Permian–Triassic boundary sections from shallow-marine carbonate platforms of the Nanpanjiang Basin, South China: implications for oceanic conditions associated with the end-Permian extinction and its aftermath. Palaios 18 (2), 138–152.
Lehrmann, D.J., Bentz, J.M., Wood, T., Goers, A., Dhillon, R., Akin, S., Xiaowei, L.I., Payne, J.L., Kelley, B.M., Meyer, K.M., 2015. Environmental controls on the genesis of marine microbialites and dissolution surface associated with the end-Permian mass extinction: new sections and observations from the Nanpanjiang Basin, South China. Palaios 30 (7), 529–552.
Li, Z., Zhan, L., Zhu, X., Zhang, J., Jin, R., Liu, G., Shen, H., Shen, G., Dai, J., Huang, H., Xie, L., Yan, Z., 1986. Mass extinction and geological events between Paleozoic and Mesozoic era. Acta Geol. Sin. ], 1–15.
Lin, J., Li, J., Sun, Q., 1990. Late Paleozoic Foraminifera in South China. Science Press,

Beijing 297 pp.
Liu, J.B., Ezaki, Y., Yang, S.R., Wang, H.F., Adachi, N., 2007. Age and sedimentology of microbialites after the end-Permian mass extinction in Luodian, Guizhou Province. J. Palaeogeogr. 9 (5), 473–486.
Loeblich, A.R., Tappan, H., 1988. Foraminiferal Genera and Their Classification. Van Nostrand Reinhold Company, New York 970 pp.
Loeblich, A.R., Tappan, H., 1992. Present status of foraminiferal classification. In: Takayanagi, Y., Saito, T. (Eds.), Studies in Benthic Foraminifera, Benthos' 90, Sendai, 1990. Tokai University Press, Tokyo, pp. 93–102.
Luo, G., Wang, Y., Algeo, T.J., Kump, L.R., Bai, X., Yang, H., Yao, L., Xie, S., 2011. Enhanced nitrogen fixation in the immediate aftermath of the latest Permian marine mass extinction. Geology 39 (7), 647–650.
Luo, G., Wang, Y., Grice, K., Kershaw, S., Algeo, T.J., Ruan, X., Yang, H., Jia, C., Xie, S., 2013. Microbial–algal community changes during the latest Permian ecological crisis: evidence from lipid biomarkers at Cili, South China. Glob. Planet. Chang. 105 (Supplement C), 36–51.
MacLeod, K.G., Quinton, P.C., Bassett, D.J., 2017. Warming and increased aridity during the earliest Triassic in the Karoo Basin, South Africa. Geology 45 (6), 483–486.
Marshall, C.R., 1990. Confidence intervals on stratigraphic ranges. Paleobiology 16 (1), 1–10.
Marshall, C.R., Ward, P.D., 1996. Sudden and gradual molluscan extinctions in the latest Cretaceous of western European Tethys. Science 274 (5291), 1360–1363.
McGhee, G.R., Clapham, M.E., Sheehan, P.M., Bottjer, D.J., Droser, M.L., 2013. A new ecological-severity ranking of major Phanerozoic biodiversity crises. Palaeogeogr. Palaeoclimatol. Palaeoecol. 370, 260–270.
McKinney, M.L., 1997. Extinction vulnerability and selectivity: combining ecological and paleontological views. Annu. Rev. Ecol. Syst. 28 (1), 495–516.
Meldahl, K.H., 1990. Sampling, species abundance, and the stratigraphic signature, of mass extinction: a test using Holocene tidal flat molluscs. Geology 18 (9), 890–893.
Meyer, K., Yu, M., Jost, A., Kelley, B., Payne, J., 2011. δ13C evidence that high primary productivity delayed recovery from end-Permian mass extinction. Earth Planet. Sci. Lett. 302 (3–4), 378–384.
Miao, L., Dai, X., Korn, D., Brayard, A., Chen, J., Liu, X., Song, H., 2019. A Changhsingian (late Permian) nautiloid assemblage from Gujiao, South China. Pap. Palaeontol. https://doi.org/10.1002/spp2.1275.
Mohtat-Aghaï, P., Vachard, D., 2005. Late Permian foraminiferal assemblages from the Hambast region (central Iran) and their extinctions. Rev. Esp. Micropaleontol. 37 (2), 205–227.
Murray, J.W., 2006. Ecology and Applications of Benthic Foraminifera. Cambridge University Press, New York 426 pp.
Nejad, M.E., Vachard, D., Siabeghodsy, A.A., Abbasi, S., 2015. Middle-Late Permian (Murgabian-Djulfian) foraminifers of the northern Maku area (western Azerbaijan, Iran). Palaeontol. Electron. 18 (1), 1–63.
Nestell, G.P., Kolar-Jurkovšek, T., Jurkovšek, B., Aljinović, D., 2011. Foraminifera from the Permian-Triassic transition in western Slovenia. Micropaleontology 57 (3), 197–222.
Nigam, R., Kurtarkar, S.R., Linshy, V., Rana, S., 2008. Response of benthic foraminifera Rosalina leei to different temperature and salinity, under laboratory culture experiment. J. Mar. Biol. Assoc. UK 88 (4), 699–704.
Novacek, M., 2001. The Biodiversity Crisis: Losing What Counts. New Press 223 pp.
Osleger, D., Read, J.F., 1991. Relation of eustasy to stacking patterns of meter-scale carbonate cycles, Late Cambrian, USA. J. Sediment. Res. 61 (7), 1225–1252.
Parker, W.C., Arnold, A.J., 2003. Quantitative Methods of Data Analysis in Foraminiferal Ecology, Modern Foraminifera. Springer Netherlands, Dordrecht, pp. 71–89.
Payne, J.L., Lehrmann, D.J., Wei, J., Orchard, M.J., Schrag, D.P., Knoll, A.H., 2004. Large perturbations of the carbon cycle during recovery from the end-Permian extinction. Science 305 (5683), 506–509.
Payne, J.L., Turchyn, A.V., Paytan, A., Depaolo, D.J., Lehrmann, D.J., Yu, M., Wei, J., 2010. Calcium isotope constraints on the end-Permian mass extinction. Proc. Natl. Acad. Sci. U. S. A. 107 (19), 8543–8548.
Payne, J.L., Summers, M., Rego, B.L., Altiner, D., Wei, J., Yu, M., Lehrmann, D.J., 2011. Early and Middle Triassic trends in diversity, evenness, and size of foraminifers on a carbonate platform in south China: implications for tempo and mode of biotic recovery from the end-Permian mass extinction. Paleobiology 37 (3), 409–425.
Peng, Y.Q., Tong, J.N., 1999. Integrated study on Permian-Triassic boundary bed inYangtze Platform. Earth Sci. 24 (1), 39–48.
Penn, J.L., Deutsch, C., Payne, J.L., Sperling, E.A., 2018. Temperature-dependent hypoxia explains biogeography and severity of end-Permian marine mass extinction. Science 362 (6419) eaat1327.
Piña-Ochoa, E., Høgslund, S., Geslin, E., Cedhagen, T., Revsbech, N.P., Nielsen, L.P., Schweizer, M., Jorissen, F., Rysgaard, S., Risgaard-Petersen, N., 2010. Widespread occurrence of nitrate storage and denitrification among Foraminifera and Gromiida. Proc. Natl. Acad. Sci. U. S. A. 107 (3), 1148–1153.
Pörtner, H.-O., 2010. Oxygen-and capacity-limitation of thermal tolerance: a matrix for integrating climate-related stressor effects in marine ecosystems. J. Exp. Biol. 213 (6), 881–893.
Pörtner, H.O., Knust, R., 2007. Climate change affects marine fishes through the oxygen limitation of thermal tolerance. Science 315 (5808), 95–97.
Pronina, G., 1988. The Late Permian foraminifers of Transcaucasus. Rev. Paléobiol. 2, 89–96.
Pronina-Nestell, G.P., Nestell, M.K., 2001. Late Changhsingian foraminifers of the northwestern Caucasus. Micropaleontology 47 (3), 205–234.
Rampino, M.R., Adler, A.C., 1998. Evidence for abrupt latest Permian mass extinction of foraminifera: results of tests for the Signor-Lipps effect. Geology 26 (5), 415–418.
Raup, D.M., 1975. Taxonomic diversity estimation using rarefaction. Paleobiology 1 (4), 333–342.
Renne, P.R., Basu, A.R., 1995. Synchrony and causal relations between permian-triassic boundary crises and siberian flood volcanism. Science 269 (5229), 1413–1416.
Risgaard-Petersen, N., Langezaal, A.M., Ingvardsen, S., Schmid, M.C., Jetten, M.S., den Camp, H.J.O., Derksen, J.W., Pina-Ochoa, E., Eriksson, S.P., Nielsen, L.P., 2006. Evidence for complete denitrification in a benthic foraminifer. Nature 443 (7107), 93–96.
Robertson, D.S., McKenna, M.C., Toon, O.B., Hope, S., Lillegraven, J.A., 2004. Survival in the first hours of the Cenozoic. Geol. Soc. Am. Bull. 116 (5–6), 760–768.
Sakagami, S., Hatta, A., 1982. On the Upper Permian Palaeofusulina-Colaniella Fauna from Khao Doi Pha Phlung, North Thailand, Geology and Palaeontology of Southeast Asia. University of Tokyo Press, pp. 1–14.
Sanei, H., Grasby, S.E., Beauchamp, B., 2012. Latest Permian mercury anomalies. Geology 40 (1), 63–66.
Saraswat, R., Nigam, R., Pachkhande, S., 2011. Difference in optimum temperature for growth and reproduction in benthic foraminifer Rosalina globularis: implications for paleoclimatic studies. J. Exp. Mar. Biol. Ecol. 405 (1), 105–110.
Schröder-Adams, C.J., Boyd, R., Ruming, K., Sandstrom, M., 2008. Influence of sediment transport dynamics and ocean floor morphology on benthic foraminifera, offshore Fraser Island, Australia. Mar. Geol. 254 (1), 47–61.
Scotese, C.R., 2001. Atlas of Earth History. University of Texas at Arlington, Department of Geology, PALEOMAP Project, Texas 58 pp.
Sepkoski, J.J., 1981. A factor analytic description of the Phanerozoic marine fossil record. Paleobiology 7 (1), 36–53.
Setoyama, E., Kaminski, M.A., Tyszka, J., 2011. The Late Cretaceous–Early Paleocene palaeobathymetric trends in the southwestern Barents Sea — palaeoenvironmental implications of benthic foraminiferal assemblage analysis. Palaeogeogr. Palaeoclimatol. Palaeoecol. 307 (1), 44–58.
Shen, Y., Farquhar, J., Zhang, H., Masterson, A., Zhang, T., Wing, B.A., 2011. Multiple S-isotopic evidence for episodic shoaling of anoxic water during Late Permian mass extinction. Nat. Commun. 2 (1), 1–5.
Shen, J., Feng, Q., Algeo, T.J., Li, C., Planavsky, N.J., Zhou, L., Zhang, M., 2016. Two pulses of oceanic environmental disturbance during the Permian–Triassic boundary crisis. Earth Planet. Sci. Lett. 443, 139–152.
Shen, S., Ramezani, J., Chen, J., Cao, C., Erwin, D., Zhang, H., Xiang, L., Schoepfer, S., Henderson, C., Zheng, Q., 2018. A sudden end-Permian mass extinction in South China. Geol. Soc. Am. Bull. 131 (1–2), 205–223.
Shen, J., Chen, J., Algeo, T.J., Yuan, S., Feng, Q., Yu, J., Zhou, L., O'Connell, B., Planavsky, N.J., 2019. Evidence for a prolonged Permian–Triassic extinction interval from global marine mercury records. Nat. Commun. 10 (1), 1563.
Sheng, J., Chen, C., Wang, Y., Rui, L., Liao, Z., Bando, Y., Ishii, K., Nakazawa, K., Nakamura, K., 1984. Permian-Triassic boundary in middle and eastern Tethys. J. Fac. Sci. Hokkaido Univ. 4 (21), 133–181.
Song, H., Tong, J., Zhang, K., Wang, Q., Chen, Z.Q., 2007. Foraminiferal survivors from the Permian-Triassic mass extinction in the Meishan section, South China. Palaeoworld 16 (1), 105–119.
Song, H., Tong, J., Chen, Z., 2009a. Two episodes of foraminiferal extinction near the Permian–Triassic boundary at the Meishan section, South China. Aust. J. Earth Sci. 56 (6), 765–773.
Song, H., Tong, J., Chen, Z., Yang, H., Wang, Y., 2009b. End-Permian mass extinction of foraminifers in the Nanpanjiang Basin, South China. J. Paleontol. 83 (5), 718–738.
Song, H., Tong, J., Chen, Z.Q., 2011a. Evolutionary dynamics of the Permian–Triassic foraminifer size: Evidence for Lilliput effect in the end-Permian mass extinction and its aftermath. Palaeogeogr. Palaeoclimatol. Palaeoecol. 308 (1–2), 98–110.
Song, H., Wignall, P.B., Chen, Z.-Q., Tong, J., Bond, D.P., Lai, X., Zhao, X., Jiang, H., Yan, C., Niu, Z., 2011b. Recovery tempo and pattern of marine ecosystems after the end-Permian mass extinction. Geology 39 (8), 739–742.
Song, H., Wignall, P.B., Tong, J., Bond, D.P., Song, H., Lai, X., Zhang, K., Wang, H., Chen, Y., 2012. Geochemical evidence from bio-apatite for multiple oceanic anoxic events during Permian–Triassic transition and the link with end-Permian extinction and recovery. Earth Planet. Sci. Lett. 353, 12–21.
Song, H., Wignall, P.B., Tong, J., Yin, H., 2013. Two pulses of extinction during the Permian-Triassic crisis. Nat. Geosci. 6 (1), 52–56.
Song, H., Wignall, P.B., Chu, D., Tong, J., Sun, Y., Song, H., He, W., Tian, L., 2014. Anoxia/high temperature double whammy during the Permian-Triassic marine crisis and its aftermath. Sci. Rep. 4 (2), 4132.
Song, H., Yang, L., Tong, J., Chen, J., Tian, L., Song, H., Chu, D., 2015. Recovery dynamics of foraminifers and algae following the Permian-Triassic extinction in Qingyan, South China. Geobios 48 (1), 71–83.
Song, H., Tong, J., Wignall, P.B., Luo, M.A.O., Tian, L.I., Song, H., Huang, Y., Chu, D., 2016. Early Triassic disaster and opportunistic foraminifers in South China. Geol. Mag. 153 (2), 298–315.
Song, H., Wignall, P.B., Dunhill, A.M., 2018. Decoupled taxonomic and ecological recoveries from the Permo-Triassic extinction. Sci. Adv. 4 (10) eaat5091.
Stanley, S., Yang, X., 1994. A double mass extinction at the end of the Paleozoic Era. Science 266 (5189), 1340–1344.
Strauss, D., Sadler, P.M., 1989. Classical confidence intervals and Bayesian probability estimates for ends of local taxon ranges. Math. Geol. 21 (4), 411–427.
Sun, Y., Joachimski, M.M., Wignall, P.B., Yan, C., Chen, Y., Jiang, H., Wang, L., Lai, X., 2012. Lethally hot temperatures during the Early Triassic greenhouse. Science 338 (6105), 366–370.
Sun, Y., Zulla, M., Joachimski, M., Bond, D., Wignall, P., Zhang, Z., Zhang, M., 2019. Ammonium ocean following the end-Permian mass extinction. Earth Planet. Sci. Lett. 518, 211–222.
Tappan, H., Loeblich, A.R., 1988. Foraminiferal evolution, diversification, and extinction. J. Paleontol. 62 (5), 695–714.
Teichert, C., Kummnel, B., Kapoor, H., 1970. Mixed Permian-Triassic fauna, Guryul

Ravine, Kashmir. Science 167 (3915), 174–175.
Tong, J., Kuang, W., 1990. A study of the Changxingian foraminifera and microfacies in Liangfengya, Chongqing, Sichuan Province. Earth Sci. J. China Univ. Geosci. 15 (3), 337–344.
Tong, J., Shi, G., Yin, H., 2000. Evolution of the Permian and Triassic foraminifera in South China. In: Dickins, J.M., Shi, G.R., Tong, J. (Eds.), Permian–Triassic Evolution of Tethys and Western Circum Pacific. Elsevier, pp. 291–307.
Vachard, D., 2016. Permian smaller foraminifers: taxonomy, biostratigraphy and biogeography. Geol. Soc. Lond. Spec. Publ. 450 (1), 205–252.
Vachard, D., Miconnet, P., 1989. Une association a fusulinoides du Murghabien superieur au Monte Facito (Apennin meridional, Italie). Rev. Micropaleontol. 32 (4), 297–318.
Vachard, D., Moix, P., 2013. Kubergandian (Roadian, Middle Permian) of the Lycian and Aladağ Nappes (Southern Turkey). Geobios 46 (4), 335–356.
Vachard, D., Pille, L., Gaillot, J., 2010. Palaeozoic foraminifera: systematics, palaeoecology and responses to global changes. Rev. Micropaléontol. 53 (4), 209–254.
Vuks, V.J., 2000. Triassic foraminifers of the Crimea, Caucasus, Mangyshlak and Pamirs (biostratigraphy and correlation). Zentralbl. Geol. Paläontol. Teil I 11-12, 1353–1365.
Vuks, V.J., 2007. Olenekian (Early Triassic) foraminifers of the Gorny Mangyshlak, eastern Precaucasus and western Caucasus. Palaeogeogr. Palaeoclimatol. Palaeoecol. 252 (1–2), 82–92.
Waldrop, M.M., 1988. After the fall: although the dust was bad, the chemical fallout from the Cretaceous-Tertiary impact was worse-much worse. Science 239 (4843), 977–978.
Wan, J., Yuan, A., Crasquin, S., Jiang, H., Yang, H., Hu, X., 2019. High-resolution variation in ostracod assemblages from microbialites near the Permian-Triassic boundary at Zuodeng, Guangxi region, South China. Palaeogeogr. Palaeoclimatol. Palaeoecol. 535, 109349.
Wang, S.C., Everson, P.J., 2007. Confidence intervals for pulsed mass extinction events. Paleobiology 33 (2), 324–336.
Wang, S.C., Marshall, C.R., 2004. Improved confidence intervals for estimating the position of a mass extinction boundary. Paleobiology 30 (1), 5–18.
Wang, Y., Ueno, K., 2009. A new fusulinoidean genus Dilatofusulina from the Lopingian (Upper Permian) of southern Tibet, China. J. Foraminifer. Res. 39 (1), 56–65.
Wang, Y., Xu, G., Lin, Q., 1997. Paleoecological relations between coral reef and sponge reef of Late Permian in Cili area, West Hunan Province. Earth Sci. 22 (2), 135–138.
Wang, Q., Tong, J., Song, H., Yang, H., 2009. Ecological evolution across the Permian/Triassic boundary at the Kangjiaping Section in Cili County, Hunan Province, China. Sci. China Ser. D Earth Sci. 52 (6), 797–806.
Wang, Y., Ueno, K., Zhang, Y.c., Cao, C.q., 2010. The Changhsingian foraminiferal fauna of a Neotethyan seamount: the Gyanyima Limestone along the Yarlung-Zangbo Suture in southern Tibet, China. Geol. J. 45 (2–3), 308–318.
Wang, L., Wignall, P.B., Wang, Y., Jiang, H., Sun, Y., Li, G., Yuan, J., Lai, X., 2016. Depositional conditions and revised age of the Permo-Triassic microbialites at Gaohua section, Cili County (Hunan Province, South China). Palaeogeogr. Palaeoclimatol. Palaeoecol. 443, 156–166.
Wignall, P.B., Hallam, A., 1996. Facies change and the end-Permian mass extinction in SE Sichuan, China. Palaios 11, 587–596.
Wignall, P.B., Twitchett, R.J., 1996. Oceanic anoxia and the end Permian mass extinction. Science 272 (5265), 1155–1158.
Wignall, P., Hallam, A., Xulong, L., Fengqing, Y., 1995. Palaeoenvironmental changes across the Permian/Triassic boundary at Shangsi (N. Sichuan, China). Hist. Biol. 10 (2), 175–189.
Winguth, A.M., Shields, C.A., Winguth, C., 2015. Transition into a Hothouse World at the Permian-Triassic boundary-A model study. Palaeogeogr. Palaeoclimatol. Palaeoecol. 440, 316–327.
Woehle, C., Roy, A.-S., Glock, N., Wein, T., Weissenbach, J., Rosenstiel, P., Hiebenthal, C., Michels, J., Schönfeld, J., Dagan, T., 2018. A novel eukaryotic denitrification pathway in foraminifera. Curr. Biol. 28 (16) 2536–2543. e5.
Wu, S., 1988. Characteristics of stratigraphical and faunal changes near the Permo-Triassic boundary in the Huayingshan area, Sichuan Province. Geoscience 2 (3), 375–385.
Wu, H., Zhang, S., Hinnov, L.A., Jiang, G., Feng, Q., Li, H., Yang, T., 2013. Time-calibrated Milankovitch cycles for the late Permian. Nat. Commun. 4, 2452.
Xie, S., Algeo, T.J., Zhou, W., Ruan, X., Luo, G., Huang, J., Yan, J., 2017. Contrasting microbial community changes during mass extinctions at the Middle/Late Permian and Permian/Triassic boundaries. Earth Planet. Sci. Lett. 460, 180–191.
Yang, Z., Yin, H., Wu, S., Yang, F., Ding, M., Xu, G., 1987. Permian-Triassic Boundary Stratigraphy and Fauna of South China. Geological Publishing House, Beijing 379 pp.
Yang, X., Jiarun, L., Guijun, S., 2004. Extinction process and patterns of Middle Permian fusulinaceans in southwest China. Lethaia 37 (2), 139–147.
Yang, H., Chen, Z., Wang, Y., Tong, J., Song, H., Chen, J., 2011. Composition and structure of microbialite ecosystems following the end-Permian mass extinction in South China. Palaeogeogr. Palaeoclimatol. Palaeoecol. 308 (1–2), 111–128.
Yang, L., Song, H., Tong, J., Chu, D., Tian, L., 2013. The extinction pattern of fusulinids during the Permian-Triassic crisis at the Ksangjiaping section, Cili, Hunan province. Acta Micropalaeontol. Sinica 30 (4), 353–366.
Yang, L., Song, H., Tong, J., Chu, D., Liang, L., Kui, W.U., Tian, L., 2016. The extinction pattern of foraminifers during the Permian-Triassic crisis at the Maochang section,Ziyun, Guizhou province, South China. Acta Micropalaeontol. Sinica 33 (3), 229–251.
Yin, H., Song, H., 2013. Mass extinction and Pangea integration during the Paleozoic-Mesozoic transition. Sci. China Earth Sci. 56 (11), 1791–1803.
Yin, H., Wu, S., 1985. Transitional Bed—the basal Triassic unit of South China. J. China Univ. Geosci. 10, 163–172.
Yin, H., Zhang, K., Tong, J., Yang, Z., Wu, S., 2001. The global stratotype section and point (GSSP) of the Permian-Triassic boundary. Episodes 24 (2), 102–114.
Yin, H., Jiang, H., Xia, W., Feng, Q., Zhang, N., Shen, J., 2014. The end-Permian regression in South China and its implication on mass extinction. Earth Sci. Rev. 137, 19–33.
Yuan, D.X., Shen, S.Z., 2011. Conodont succession across the Permian-Triassic boundary of the Liangfengya section, Chongqing, south China. Acta Palaeontol. Sin. 50 (4), 420–438.
Yuan, D.-x., Chen, J., Zhang, Y.-c., Zheng, Q.-f., Shen, S.-z., 2015. Changhsingian conodont succession and the end-Permian mass extinction event at the Daijiagou section in Chongqing, Southwest China. J. Asian Earth Sci. 105, 234–251.
Yuan, D.-X., Shen, S.-z., Henderson, C.M., Chen, J., Zhang, H., Zheng, Q.-f., Wu, H., 2019. Integrative timescale for the Lopingian (Late Permian): a review and update from Shangsi, South China. Earth Sci. Rev. 188, 190–209.
Zhang, M., 2015. Late Permian Deep Water Foraminifal Fauna from South China. Ph.D. Thesis. China University of Geosciences, Wuhan 171 pp.
Zhang, M., Gu, S., 2015. Latest Permian deep-water foraminifers from Daxiakou, Hubei, South China. J. Paleontol. 89 (3), 448–464.
Zhang, Y.C., Yue, W., 2017. Permian fusuline biostratigraphy. In: Lucas, G.S., Shen, S.Z. (Eds.), The Permian Timescale. Geological Society, London, pp. 253–288.
Zhang, K., Tong, J., Yin, H., Wu, S., 1996. Sequence stratigraphy of the Permian-Triassic boundary section of Changxing, Zhejiang. Acta Geol. Sin. 70 (3), 270–281.
Zhang, Y.-C., Wang, Y., Zhang, Y.-J., Yuan, D.-X., 2013. Artinskian (Early Permian) fusuline fauna from the Rongma area in northern Tibet: palaeoclimatic and palaeobiogeographic implications. Alcheringa Australas. J. Palaeontol. 37 (4), 529–546.
Zhang, Y.-c., Shen, S.-z., Zhang, Y.-j., Zhu, T.-x., An, X.-y., 2016. Middle Permian non-fusuline foraminifers from the middle part of the Xiala Formation in Xainza county, Lhasa Block, Tibet. J. Foraminifer. Res. 46 (2), 99–114.
Zheng, Z., 1981. Uppermost Permian (Changhsingian) ammonoids from Western Guizhou. Acta Palaeontol. Sin. 20 (2), 107–113.